Measuring dc electric fields using second harmonic generation in a centro-symmetric gas

Diploma paper

Magnus Buhrgard
Mats Jönsson

PREFACE

This paper deals with second harmonic generation (SHG) in centro-symmetric gases, especially in SF_6, when applying a dc electric field between two electrodes in the gas. This method could prove to be a way of measuring the electric field strength without having to use a probe and possibly even receiving a 3-dimensional resolution of the field.

The idea was initiated by ASEA RESEARCH, and the experiments were carried out in Lund, at the Department of Atomic Physics at Lund Institute of Technology, during 1985. Other possible methods have been considered and explained theoretically in the text, but no experiments were carried out using these methods.

Our joint diploma work is constituted of the construction of a measurement cell, experiments and an evaluation of the method. The first chapter is an introduction to this paper while the second chapter deals with the theory of SHG and the approximations necessary to calculate the field strength between the electrodes. A theoretical summary of other possible methods is given in chapter three.

The experiments are described and the results are given in the fourth chapter, while an evaluation of them is given, and experimental improvements are suggested in the next chapter. This is followed by a summary and appendices. In the appendices one finds the drawings of the measurement cell and various graphs.

We would like to take the opportunity to thank our supervisor, Anders Persson, M.Eng.Sc., for his advice and support as well as Dr. Arne Hjortsberg and Dr. Sven Hörnfeldt at ASEA RESEARCH for their advice and help in outlining this project.

LUND, OCTOBER 1985

Magnus Buhrgard
Mats Jönsson

CONTENTS

Page

CHAPTER 1: INTRODUCTION

1.1. Intentions

Our intentions with this joint diploma work have been several

* to design a measurement cell for SHG measurements of dc electric fields in a gas.

* to find an experimental arrangement in which the generated SHG can be detected.

* to carry out experiments with SF_6 and verify the formulae approximately describing the electric field strength when using cylindrical electrodes.

* to give a short theoretical summary of methods other than SHG that might prove of use when measuring dc electric fields, without a probe.

The idea was raised by ASEA RESEARCH because gas insulation is used in HVDC (high voltage direct current) equipment. SHG could prove to be a useful method when measuring electric fields without having to use a probe. Theoretically it is possible to get a 3-dimensional resolution of the field strength. The choice of SF_6 was based on the fact that the effect (SHG) is stronger in SF_6 than in most other centrosymmetric gases, and that ASEA use this gas commercially in their equipment.

1.2. Objectives

Our objectives have been, following the points above, to construct a measurement cell in which different types of electrodes can be fixed and connected to high tension (0-12 kV). The drawings of the cell can be found i appendix IV.

After constructing the cell the task was to find a suitable experimental arrangement, able to detect the frequency doubled signal. Once having found the signal, the objective was to verify the approximations (references [6] and [7]) giving the electric field strength and from this point evaluate the possibilities of the method, i.e., if it is useful for measuring electric fields in gases. Improvements in the design of the measurement cell, experimental arrangements etc. are to be considered and suggested.

The last objective was to give a short specification, from a theoretical point of view, of other methods that might prove to be applicable or already have proven to be. Among these are two particularly interesting methods

* refractive index change, which has been used by Anders Persson.

* local modulation of the dielectric constant, which has been tried out by Dr. Stig Borgström.

CHAPTER 2: THEORETICAL ASPECTS OF SHG

A useful property of nonlinear optical phenomena is that they provide methods of extending the available frequency range for lasers. In this chapter we will discuss second harmonic generation (SHG). Specifically, SHG has proved to be a useful method, with a fairly high degree of efficiency, especially when using liquids and crystals. It is also possible to get SHG in nonsymmetric gases, and if one applies a dc electric field, SHG is possible in symmetric gases as well. Part of the theory necessary to aquire a better understanding of SHG and, to some extent, the experimental results when using a centro-symmetric gas, like SF_6, will be given here. The application of a dc electric field, using a centro-symmetric gas, makes approximations necessary. Therefore part of this chapter will be reserved for these aspects as well as the properties of SF_6.

The interest given to SHG in symmetric gases is based on the possibility of using this phenomenon (method) when measuring electric field strength. Theoretically it is possible to achieve a 3-dimensional resolution of the field distribution. This is done by moving the focus of the generating beam, and achieved because of the SHG signal's quadratic dependence on the laser's intensity. In the focal plane of the generating beam one gets a well defined volume of generation, if the beam used is convergent. In order to generate the second harmonic, the material is excited using a high-power pulsed laser. In this case a Q-switched Nd:YAG laser was used. When high laser intensities are used, an optical wave of twice the fundamental frequency emerges. This is due to the nonlinear optical polarization of the medium. Normally, SHG is not achievable in a system with inversion symmetry. The inversion symmetry is broken up if one applies a dc electric field.

2.1. Introductory Theory

In classical linear optics one assumes that the induced dielectric polarization, the dipole moment per unit volume, of a medium is linearly related to the applied electric field, i.e.

$$\underline{P} = \varepsilon_0 \chi \underline{E} \qquad [1]$$

where χ $(=\varepsilon_r - 1)$ is the dielectric susceptibility and ε_r is the permittivity of the medium. The presence of strong electric fields, as is the case when using high-power lasers, give rise to nonlinearities in the polarization. Thus the above relation (1) is no longer valid and serves only as a crude approximation of the situation at hand. One has to consider further terms of $\underline{P}$, which are related to higher powers of $\underline{E}$. This nonlinear response can lead to an exchange of energy between

electromagnetic waves at different frequencies. We can write

$$P = \varepsilon_0 \chi_1 E + \varepsilon_0 \chi_2 E^2 + \varepsilon_0 \chi_3 E^3 + \ldots \quad [2]$$

where χ_i is the coefficient of polarizability (susceptibility).

These nonlinear effects can be studied in a crystal, e.g. KDP, exposed to a high-power laser beam. The propagation of light in a transparent medium can be looked upon as a process in which electric dipoles, electrones bound to a nucleus, are put into oscillation by the radiation field and then reradiate the light. As long as the amplitude of oscillation is small the dipoles can follow the oscillation in detail, but as the amplitude increases, the nonlinear effects become non-negligible. The nonlinear effects arise when the dipoles cannot reproduce the forced oscillation which leads to generation of harmonics.

Now, let us assume that the induced nonlinear polarization $\underline{P}^{NL}$ is related to the electric field $\underline{E}$ of the electromagnetic wave by a scalar equation, i.e.

$$P^{NL} = 2\varepsilon_0 d\, E^2 \quad [3]$$

where d is a coefficient whose dimension is the inverse of the electric field. The physical origin of [3] is as stated above, due to the nonlinear deformation of the outer, loosely bound electrons of an atom or atomic system when subjected to high electric field strengths. A comparison of [1] and [3] shows that the nonlinear polarization term becomes comparable to the linear one for a certain electric field. We then find that (1/d) must be that field strength at which a sizeable nonlinear deformation of the outer electrons will occur,i.e., the linear and nonlinear terms become comparable. We note that for symmetry reasons, d must be zero for a centro-symmetric material (such as for a centro-symmetric crystal and usually for liquids and gases as well). Let us now consider a monochromatic plane wave of frequency ω propagating in the z direction through a nonlinear crystal. For a plane wave of uniform intensity we can write the following expression for the electric field $E_\omega(z,t)$ of the wave

$$E_\omega(z,t) = E(z,\omega)\cos(\omega t - kz) \quad [4]$$

$$k_\omega = \omega/c_\omega = \omega n_\omega/c_0 \quad [5]$$

where c is the velocity of light in the crystal, n_ω is the refractive index at frequency ω, and c_0 is the velocity of light in vacuum. Substitution of [4] into [3] shows that the nonlinear polarization P^{NL} contains a constant term as well as a term oscillating at frequency 2ω, namely

$$P^{NL} = 2\varepsilon_0 d\, E^2(z,\omega)\cos^2(\omega t - k_\omega z) = \varepsilon_0 d\, E^2(z,\omega)\{1+\cos(2\omega t - 2k_\omega z)\} \quad [6]$$

Equation [6] describes a polarization oscillating at frequency 2ω and whose spatial variation is in the form of a wave at the second harmonic frequency, 2ω, and this wave has the form

$$E_{2\omega}(z,t) = E(z,2\omega)\cos(2\omega t - k_{2\omega} z) \quad [7]$$

$$k_{2\omega} = 2\omega/c_{2\omega} = 2\omega n_{2\omega}/c_0 \quad [8]$$

Here, $k_{2\omega}$ is the magnitude of the wave vector at frequency 2ω.

The physical origin of SHG can thus be traced back to the fact that, as a result of the nonlinear relation [3], the e.m. wave at the fundamental frequency ω will beat with itself to produce a polarization at 2ω. A comparison of [6] with [7] reveals a very important condition which must be satisfied if this process is to occur efficiently, viz., that the phase velocity of the polarization wave ($v_P = 2\omega/2k_\omega$) must be equal to that of the generated e.m. wave ($v_E = 2\omega/k_{2\omega}$). The condition can thus be written

$$k_{2\omega} = 2k_\omega \quad [9]$$

In fact, if this condition is not satisfied, the phase ($2k_\omega l$) of the polarization wave at some point a distance l into the crystal will be different from that of the generated wave ($k_{2\omega} l$). This increasing phase difference with distance l means that the generated wave will not grow cumulatively with distance l since it is not being driven by a polarization with the appropriate phase. Condition [9] is therefore referred to as the <u>phase-matching condition</u>. Note, that according to [5] and [8], equation [9] reduces to

$$n_{2\omega} = n_\omega \quad [10]$$

If the directions of E_ω and P^{NL} (and hence of $E_{2\omega}$) were indeed the same (as implied by [2]) it would not be possible to satisfy the condition [10] owing to the dispersion ($\Delta n = n_{2\omega} - n_\omega$) of the crystal. This would then set a severe limit to the crystal length, l_c, for which P^{NL} can give contributions which keep adding cumulatively to form the second harmonic wave. This length l_c, the coherence length, must in fact correspond to the distance over which the P wave and the $E_{2\omega}$ wave get out of phase with each other by an amount of π, i.e.,

$$k_{2\omega}l_c - 2k_{\omega}l_c = \pi \qquad [11]$$

From this, with the help of [5] and [8], we get

$$l_c = \lambda/4\Delta n \qquad [12]$$

where $\lambda = 2\pi c_0/\omega$ is the wavelength in vacuum of the fundamental wave. If we visualize the SHG process in terms of photons we find that

$$\hbar\omega_{SH} = 2\hbar\omega \qquad [13]$$

$$\hbar k_{SH} = 2\hbar k_{\omega} \qquad [14]$$

Equation [13] states the conservation of photon energy while relation [14] corresponds to the requirement that photon momentum also should be conserved in the process.

In an anisotropic crystal it can be shown that, for a given direction of propagation, there are two different linearly polarized plane waves which can propagate. Corresponding to these two different polarizations there are two different refractive indices.

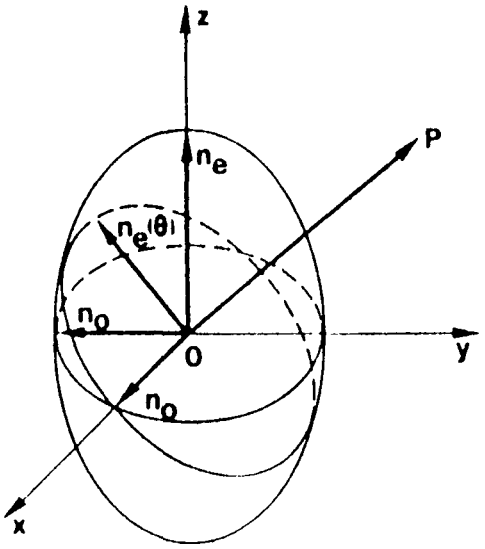

Fig.1. Index ellipsoid for a positive uniaxial crystal.

The difference of refraction index is referred to as birefringence. This behaviour is usually described in terms of the so called index ellipsoid of revolution around the optic axis (z axis of Fig.1.). The wave having polarization perpendicular to the optic axis is called the ordinary wave. Its refractive index n_0 can be seen from the figure to be independent of the direction of propagation. If the polarization is parallell to the optic axis the wave is called extraordinary and the corresponding index of refraction $n_e(\theta)$ ranges in value from that of n_0 to a value n_e, called the extraordinary index (when OP is perpendicular to z).

A positive uniaxial crystal corresponds to the case $n_e > n_0$ and the opposite case (i.e. $n_0 > n_e$) is refered to as negative uniaxial crystal. In general, in an anisotropic medium, the scalar relation [3] does not hold and a tensor relation needs to be introduced. A thorough discussion can be found in references [2] and [5], we can write

$$P_z = 2\varepsilon_0 d\, E_x E_y \quad \text{(permutate to get } P_x, P_y) \qquad [15]$$

where the z axis is again taken along the optic axis of the uniaxial crystal. From [15] we note that, if $E_z=0$, only P_z will be nonvanishing and will thus tend to generate a second harmonic wave with a nonzero z component. We recall (see fig.1.) that a wave with $E_z=0$ is an ordinary wave while a wave with $E_z \neq 0$ is an extraordinary wave. Thus, an ordinary wave at the fundamental frequency ω tends to, in this case, generate an extraordinary wave at 2ω. To satisfy the phase-matching condition one can then direct the fundamental wave at an angle Θ_m to the optic axis, in such a way that

$$n_e(2\omega, \Theta_m) = n_0(\omega) \qquad [16]$$

From the equation of an ellipse $\{1/r^2 = (a/x)^2 + (b/y)^2\}$ one gets the phase-matching condition

$$1/n^2 = (\cos\Theta/n_0)^2 + (\sin\Theta/n_e)^2 \qquad [17]$$

This can be better understood with the help of fig.2. which shows the intercepts of the normal surfaces $n_0(\omega)$ and $n_e(2\omega, \Theta)$ with the plane containing the z axis and the propagation direction.

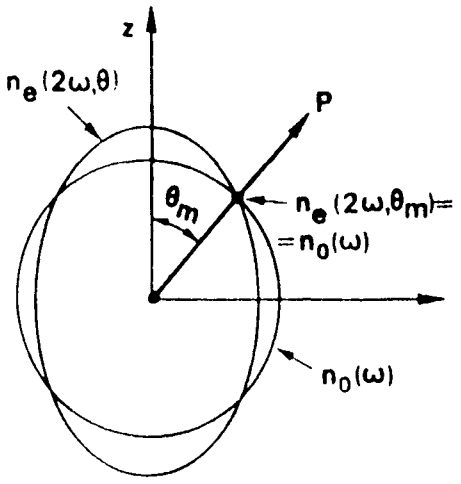

Fig.2. Phase-matching angle Θ_m for type I SHG in a negative uniaxial crystal.

Note that, due to the dispersion, we have $n_o(\omega) < n_o(2\omega) = n_e(2\omega,0)$. Thus the ordinary circle (for frequency ω) intersects the extraordinary ellipse (for frequency 2ω) at some angle θ_m. For light propagating at this angle θ_m to the optic axis (i.e. for all ray directions lying in a cone around the z axis, with cone angle θ_m), equation [15] is satisfied and hence the phase-matching condition is satisfied. Note, however, that if $\theta \neq 90^\circ$ the phenomenon of double refraction will occur, i.e., the direction of the energy flow for the extraordinary (SH) beam will be at an angle slightly different from θ_m. Thus the fundamental and SH beams will travel in slightly different directions (although satisfying the phase-matching condition).

For a fundamental beam of finite transverse dimensions this will put an upper limit on the interaction length in the crystal. This limitation can be overcome if it is possible to operate with $\theta_m = 90^\circ$, i.e., $n_e(2\omega,90^\circ) = n_o(\omega)$. This kind of phase-matching is called 90° phase-matching and can, in some cases, be acheived by changing the crystal temperature, since n_e and n_o in general undergo different changes with the temperature. To summarize the above discussion we can say that phase-matching can be acheived in a (sufficiently birefringent) negative uniaxial crystal when an ordinary ray at ω (E_x beam of [15]) combines with an ordinary ray at ω (E_y beam of [15]) to give an extraordinary ray at 2ω. This is called type I SHG. In a negative uniaxial crystal another scheme for phase-matched SHG, called type II, is also possible. In this case an ordinary wave at ω can combine with an extraordinary wave at ω to give an extraordinary wave at 2ω.

2.2 Analytical Treatment of SHG

To arrive at an analytical description of SHG, one needs to see how the nonlinear polarization [2], which acts as the source term to drive the generated waves, is introduced into the wave equation. The fields within the material obey Maxwell's equations

$$\text{curl } \underline{E} = -\partial_t \underline{B} \qquad [18]$$

$$\text{curl } \underline{H} = \underline{J} + \partial_t \underline{D} \qquad [19]$$

$$\text{div } \underline{D} = \rho \qquad [20]$$

$$\text{div } \underline{B} = 0 \qquad [21]$$

where ρ is the free-charge density.

For the medium of interest here, we can assume the magnetization $\underline{M}$ to be zero, thus

$$\underline{B} = \mu_0\underline{H} + \mu_0\underline{M} = \mu_0\underline{H} \qquad [22]$$

Losses within the material, i.e. scattering losses, can be simulated by the introduction of a fictitious conductivity σ_s, such that

$$\underline{J} = \sigma_s\underline{E} \qquad [23]$$

Finally we can write

$$\underline{D} = \varepsilon_0\underline{E} + \underline{P}^L + \underline{P}^{NL} = \varepsilon\underline{E} + \underline{P}^{NL} \qquad [24]$$

where $\underline{P}^L$ is the linear polarization of the medium and is taken account of, in the usual way, by introducing the dielectric constant ε. When $\underline{D}$, given by [24], is substituted in Maxwell's equations, the nonlinear polarization term $\underline{P}^{NL}$ is introduced into the wave equation. Applying the curl operator to both sides of [18] , interchanging the curl and ∂-operators on the right hand side of [18], and making use of [22], [19] ,[23] and [24] we obtain the wave equation with the nonlinear polarization term included, assuming that div $\underline{E} \approx 0$.

$$\text{div grad } \underline{E} - \sigma_s/\varepsilon c^2\ \partial_t^2\underline{E} - 1/c^2\ \partial_t\underline{E} = 1/\varepsilon c^2\ \partial_t^2\underline{P}^{NL} \qquad [25]$$

where $c = 1/\sqrt{\varepsilon\mu_0}$ is the phase velocity in the material. Note that the linear part of the polarization has been transferred to the left-hand side of [25] and is contained in the dielectric constant ε. The nonlinear part, $\underline{P}^{NL}$, has been kept on the right-hand side, and it can be shown to act as a source term for the waves being generated at new frequencies as well as a loss term for the incoming wave, see reference [5] for a thorough analysis.

Assume that we have a simple scalar case of plane waves propagating along the z-direction, this reduces [24] to

$$\partial_z^2 E - \sigma_s/\varepsilon c^2\ \partial_t E - 1/c^2\ \partial_t^2 E = 1/\varepsilon c^2\ \partial_t^2 P^{NL} \qquad [26]$$

The field amplitude at frequency ω_j can be expressed as

$$E^{\omega j}(z,t) = E_j(z)\ \cos(\omega_j t - k_j z) \qquad [27]$$

where E_j in general is a complex function.

Likewise, the amplitude of the nonlinear polarization at frequency ω_j can be expressed as

$$P^{NL}_{\omega j} = P^{NL}_j(z)\cos(\omega_j t - k_j z) \qquad [28]$$

Since [26] must hold seperately for each frequency corresponding to waves which are present in the crystal, equations [27] and [28] can be substituted into the left- and right-hand sides of [26], respectively within the slowly varying amplitude approximation, we can neglect the second derivative of $E_j(z)$, i.e. assume that $d^2E/dz^2 \ll k_j(dE_j/dz)$, this then yields

$$2\,dE_j/dz + (\sigma_j/n_j\varepsilon_0 c_0)\,E_j = -i(\omega_j/n_j\varepsilon_0 c_0)\,P^{NL}_j \qquad [29]$$

where the relations $k_j = n_j\omega_j/c_0$ and $\varepsilon_j = n_j\varepsilon_0$ have been used, n_j is the refractive index at ω_j. Note that [29] has been obtained subject to the assumption of a scalar relation between $\underline{P}^{NL}$ and $\underline{E}$. This assumption is not correct and, as has been mentioned before, actually a tensor relation should be used.

In the case of SHG we take

$$E(z,t) = 1/2\,\{E_\omega\exp[i(\omega t - k_\omega z)] + E_{2\omega}\exp[i(2\omega t - k_{2\omega} z)] + cc.\} \qquad [30]$$

$$P(z,t) = 1/2\,\{P^{NL}_\omega\exp[i(\omega t - k_\omega z)] + P^{NL}_{2\omega}\exp[i(2\omega t - k_{2\omega} z)] + cc.\} \qquad [31]$$

where cc. is the complex conjugate.

Substituting [30] and [31] into [3] and then substituting the two resulting expressions into [28] and neglecting crystal losses (i.e. putting $\sigma_j = 0$), we obtain the basic equations describing SHG.

$$d_z E_{2\omega} = -i\omega d/n_{2\omega} c_0\, E^2_\omega \exp(i\Delta k z) \qquad [32]$$

$$d_z E_\omega = -i\omega d/n_\omega c_0\, E_{2\omega} E^*_\omega \exp(-i\Delta k z) \qquad [33]$$

where $\Delta k = k_{2\omega} - 2k_\omega$.

When solving these equations one finds that they are coupled through a single parameter, l_{SH}.

$$l_{SH} = \lambda_0\sqrt{n_\omega n_{2\omega}}/2\pi d E_\omega(0) \qquad [34]$$

where l_{SH} is a characteristic length for the second harmonic interaction, λ_0 is the wavelength and $E_\omega(0)$ is the incident field amplitude of the fundamental wave at frequency ω. We find that

$$d|E_{2\omega}|^2/dz = -\sqrt{(n_\omega/n_{2\omega})}\; d|E_\omega|^2/dz \text{ (Manley-Rowe relation)} \quad [35]$$

According to this relation, it is possible in this case to have 100% conversion of fundamental beam power into second harmonic power. As a first example of the solution of [32] and [33] (a fairly complete analysis is made in reference [5]), we consider the case where there is an appreciable phase mismatch (by which we mean $\Delta k l_{SH} >> 1$) so that little conversion of fundamental into SH is expected to occur. After some manipulations one gets

$$|E_{2\omega}(l)/E_\omega(0)|^2 = (n_\omega/n_{2\omega})\; \{\sin[\Delta k l/2]/(\Delta k l_{SH}/2)\}^2 \quad [36]$$

Since $|E_{2\omega}|^2$ is proportional to the SH intensity $I_{2\omega}$, the variation of this intensity with crystal length is readily obtained from [36]. According to the Manley-Rowe relation the behaviour of I_ω must then be such that $I_\omega + I_{2\omega} = I_\omega(0)$. The dependence of $[I_\omega/I_\omega(0)]$ and $[I_{2\omega}/I_\omega(0)]$ on (l/l_{SH}) for $l_{SH}\Delta k = 10$ have both been plotted as dashed curves in fig.3. Note that, due to the large phase mismatch, only little conversion to SH occurs. It can readily be shown from [36] that the first maximum of $[I_{2\omega}/I_\omega(0)]$ occurs at $l = l_c$ where l_c (the coherence length) is given by [12].

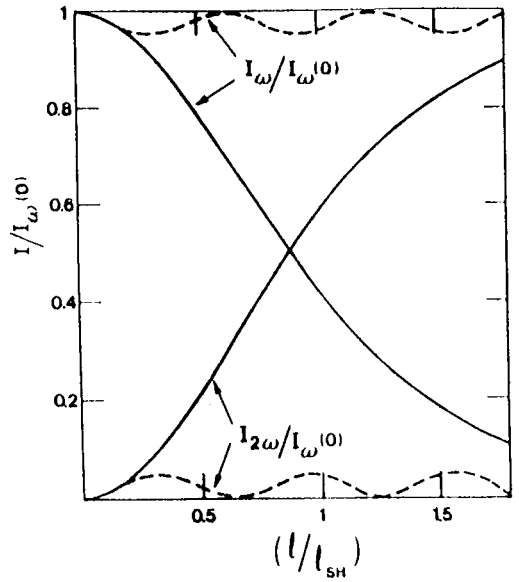

Fig.3. Normalized plots of SH intensity $I_{2\omega}$ and fundamental intensity I_ω versus crystal length l for perfect phase-matching (continuous curves) and for a finite phase mismatch (dashed curves).

As a second example of the solution to [32] and [33], we consider the case of perfect phase-matching ($\Delta k = 0$). In this case appreciable conversion to SH may occur and the depletion of the fundamental beam must therefore be considered.

We get the equations

$$d|E_\omega|/\,dz = -\sqrt{n_{2\omega}/n_\omega}\,\{|E_{2\omega}||E_\omega|/\,l_{SH}E_\omega(0)\} \quad [37]$$

$$d|E_{2\omega}|/dz = \sqrt{n_\omega/n_{2\omega}}\,\{|E_\omega|^2\,/\,l_{SH}E_\omega(0)\} \quad [38]$$

The solution of [37] and [38] with the boundary conditions $E_\omega(l=0) = E_\omega(0)$ and $E_{2\omega}(0) = 0$ is

$$E_{2\omega} = \sqrt{n_\omega/n_{2\omega}}\;E_\omega(0)\,\tanh(z/l_{SH}) \quad [39]$$

$$E_\omega = E_\omega(0)\,\mathrm{sech}(z/l_{SH}) \quad [40]$$

The dependence of $I_{2\omega}/\,I_\omega(0)$ and $I_\omega/\,I_\omega(0)$ on crystal length as predicted by [39] and [40] is shown by the solid curve in fig. 3. Note that, for $l=l_{SH}$, an appreciable fraction ($\approx$59%) of the incident wave has been converted into SH. Note also that for $l>>l_{SH}$ the fundamental radiation can be completely converted into SH radiation, in agreement with the Manley-Rowe relation.

2.3. Properties of SF_6

Sulphurhexafluoride, SF_6, is a colourless, odourfree, nonpoisonous and inactive gas. It is about five times heavier than air and is one of the heaviest gases known. SF_6 is used as insulating and cooling medium in electric devices but it is frequently used as arc-extinguishing medium in contact breakers as well. When used as described, it is desirable to know some of its technical properties.

The dielectric constant, ε, at 20° C, normal pressure and 23.34 MHz is

$$\varepsilon = 1.0021$$

Another property, that could be useful to be aware of is the solubility in different media

* in water at 25.5° C: 1 ml/l

* in transformer oil at 25° C: 300 ml/l

It is, or at least it can be, important to realize that SF_6 cannot be produced with a 100% degree of purity. There will always be traces of pollutants, such as O_2 N_2, CF_4, S_2F_{10}, SO_2 and H_2O, all in various quantaties) of which some are toxic. If one has liquified SF_6 and requires absolutely dry SF_6, it is necessary to tap the gas from the bottom of the gas holder.

Used at temperatures below 150° C SF_6 is absolutely inactive while at temperatures above 150° C the presence of water or contact material has a dissolving function on SF_6. The stable chemical properties of SF_6 can be explained by the atomic structure of sulphur. It is possible to remove two valence electrons with a small amount of energy, 2·15.9 eV. One then gets six free bonds with which the fluorine atoms can bond in an octahedral arrangement.

The thermal dissociation of SF_6 starts at temperatures above 500° C, but if one cools the gas it will recombine with the exception of only a small fraction, which will instead react with the vapourized electrode material and then form metal fluorides, e.g. when one has a voltaic arc.

A breakdown in SF_6 does not occur until the field strength exceeds

$$E/p = (E/p)_0 \approx 89 \text{ kV/cm bar}$$

according to theoretical calculations for a continous voltage, while the corresponding value in air is 27 kV/cm bar. The field strength is proportional to the pressure, thus one gets

$$E_0 = (E/p)_0 \cdot p \qquad [41]$$

These values are, as said before, theoretical and in practice one will of course get a breakthrough for a smaller field intensity. The actual breakthrough level depends, among many things, on the irregularity of the electrode surface. The breakdown will occur at different field intensities depending on what type of voltage is used. Mosch and Hauschild has, through experiments, developed a formula giving the field intensity for breakdown

$$E_d(p) = (E_d/p) \cdot p^z \qquad [42]$$

Type of voltage	E_d/p [kV/cmbar]	z
DC- or AC-voltage (SF_6)	65	0.73
Theoretical values (SF_6)	89	1.00

Table 1.

Having the same electrode distance, a, one gets a breakdown earlier when one has an electrode configuration giving an inhomogeneous electric field than when one gets a homogeneous one.

The breakthrough voltage for different electrode configurations in both air and SF_6 as a function of electrode distance can be found in fig.4. and fig.5.

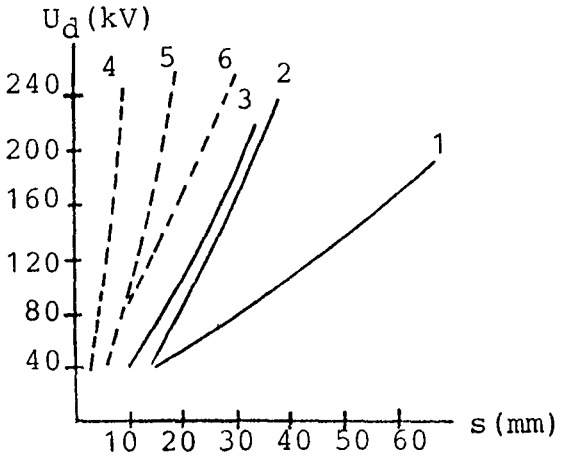

Fig.4. The breakthrough voltage U , when applying a 50Hz field, as a function of electrode distance.

Air: curves 1,2,3
SF_6: curves 4,5,6

Curves 1,4: plate-plate electrodes
Curves 2,5: sphere-plate electrodes
Curves 3,6: point-plate electrodes

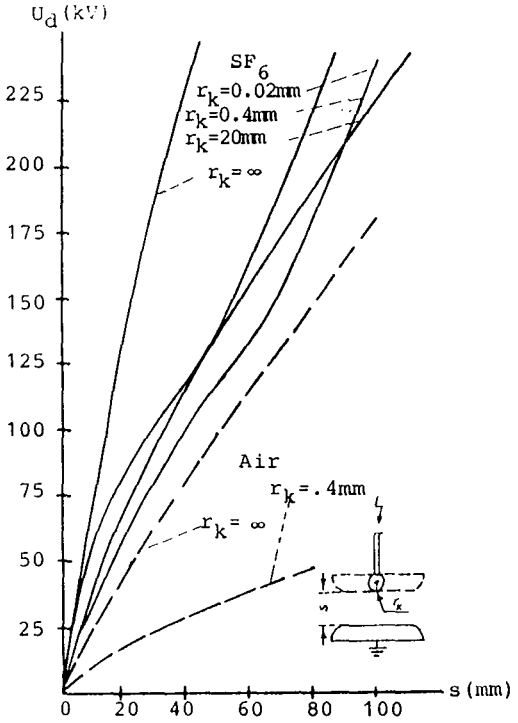

Fig.5. Breakthrough voltage in SF_6 at normal pressure as a function of electrode shape and electrode distance.

The refractive index of SF_6 at normal pressure (see ref. [10]) can be found in fig.6. where $(n-1)\cdot 10^6$ has been plotted as a function of λ, the wavelength.

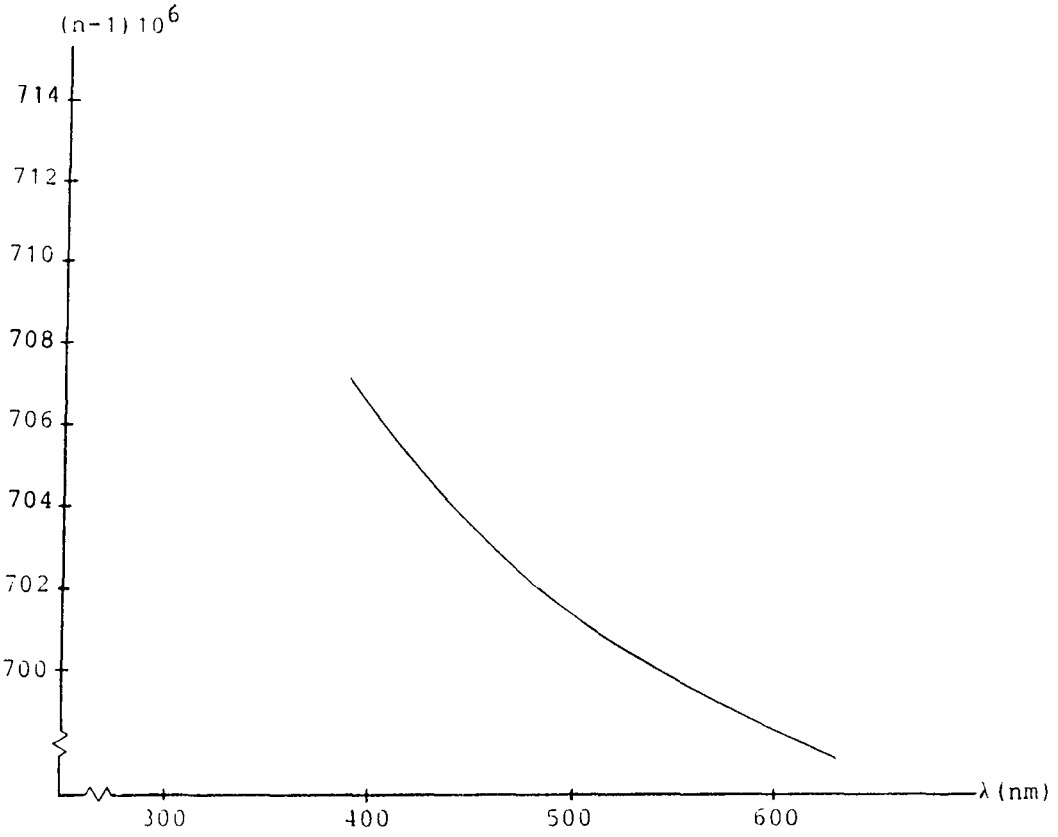

Fig.6. Refractive index of SF_6 as a function of λ.

2.4 Approximations when applying a dc electric field

As we have stated before, a centro-symmetric system does not usually generate second harmonic. However, when subjected to a dc electric field $\underline{E}^0$, and an optical field $\underline{E}^{\omega}$ at frequency ω a system, even if centro-symmetric, develops a dipole moment $\underline{P}^{2\omega}$ at the second harmonic frequency which subsequently radiates. This process is known as dc electric field-induced SHG.

In references [6] and [7] one finds the approximations necessary, to calculate $\underline{E}^0$, when using a pair of cylindrical electrodes whose geometry and dimensions are shown i fig. 7.

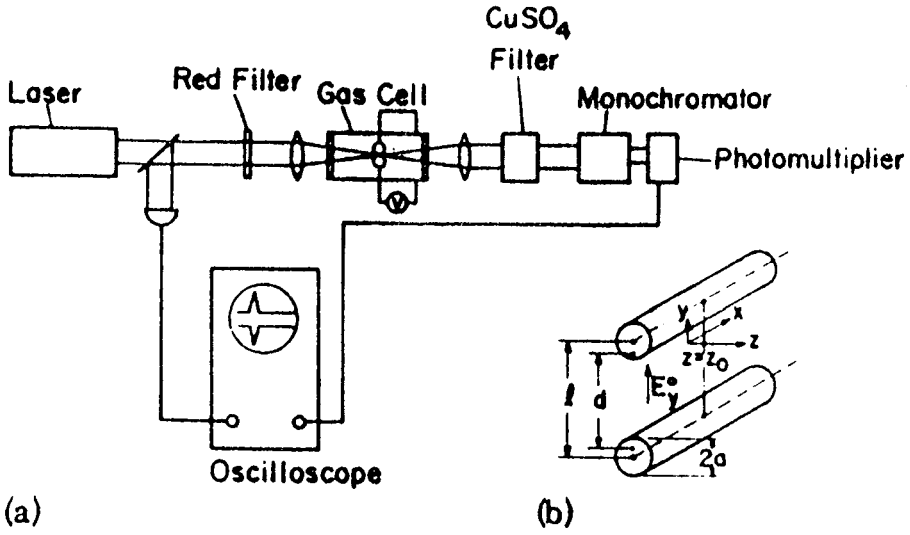

Fig.7. (a) Schematic diagram of the apparatus used in references [6] and [7].
(b) Electrode geometry.

If $\underline{E}^0$ is chosen to be in the y-direction and $\underline{E}^\omega$ in the xy-plane, $P_y^{2\omega}$ for a spherically symmetric system, such as an inert gas atom, can be written

$$P^{2\omega} = 3/2\ \chi_{yyyy}(-2\omega;o,\omega,\omega)E_y^0E_y^\omega E_y^\omega + 3/2\ \chi_{yyxx}(-2\omega;o,\omega,\omega)E_y^0E_y^\omega E_x^\omega \qquad [43]$$

We have thus managed to relate $P^{2\omega}$, the SH power, to χ_{ijkl}, the atomic coefficient for dc-induced SHG.

There are only two independent coefficients and these may be chosen to be $\chi_{yyyy}(-2\omega;0,\omega,\omega)$ and $\chi_{yyxx}(-2\omega;0,\omega,\omega)$. The ratio between these coefficients

$$R = \chi_{yyyy}(-2\omega;0,\omega,\omega)/\chi_{yyxx}(-2\omega;0,\omega,\omega) \qquad [44]$$

has been measured for a number of gases. These values of R do not significantly differ from 3.0, which is the theoretical value, i.e.,

$$\lim_{\omega \to 0} R = 3.0$$

which implies that there is negligible dispersion of $\chi_{ijkl}(-2\omega;0,\omega,\omega)$. When measuring SF_6 one obtained R= 2.97 ± 0.07, see ref. [6] and [7].

$P^{2\omega}$ could also be interpreted as the induced dipole moment amplitude per molecule where χ_{ijkl} then would mean the effective molecular hyperpolarizability. The E's are electric field amplitudes at frequencies indicated by superscripts. Now, let us designate χ_{yyyy} by $\chi_{\parallel}$ and χ_{yyxx} by $\chi_{\perp}$, referring to components measured with the optical field respectively parallel and perpendicular to the dc field. Because of the value of R we realize that even though we get a signal whichever way the incoming optical wave is polarized, the signal will be the strongest when the laser beam is polarized parallel to the applied field.

Now, let us get back to the main topic of this section, the necessary approximations. We assume that the laser beam is taken to be a lowest order Gaussian mode with a wave vector $\hat{z}k^{\omega}$, confocal parameter b and a beam-waist located at the coordinate origin (see fig.7.). The wave vector mismatch, Δk, is defined by

$$\Delta k = k_{2\omega} - k_{\omega} \qquad [45]$$

and is negative and small compared to k^{ω}, Δk^{0} will be used to indicate the wave vector mismatch at STP (standard temperature and pressure). The transverse dc electric field $E^{0}(z)$ in the region of the beam is given, to a good approximation, by

$$E_y^0(z) = \{2V/[d \cdot \cosh^{-1}(1/2a)]\} \cdot \{1/1+[2(z-z_0)/d]^2\} \qquad [46]$$

where $d^2 = l^2-4a^2$, l is the distance between the electrode axes, V is the applied dc-voltage, a is the radius of the cylindrical electrodes and z is the distance from origin, z_0. The approximation depends on the optical beam-waist diameter being small compared to d and its far field diffraction angle being small as well. The distance between equivalent thin electrodes, d, is also a measure of the extent of the field in the z-direction. According to reference [6] one gets

$$P^{2\omega} = (P^{\omega})^2 (E_y^0(z_0))^2 (36\pi^4 L^2 \omega^3 / e^2 c^4)[\chi/\Delta k_0]\ 1/d\ \Gamma(\rho)B(b)Z(z_0) \qquad [47]$$

where

$$\Gamma(\rho) = [\rho/\rho_0 \exp\{-(\rho-\rho_0)/\rho\}\ ]^2 \qquad [48]$$

and $\rho_0 = 2/d|\Delta k_0|$ is the optimum relative density, which is the density that makes the coherence length in the gas equal to $\pi d/2$.

The second factor

$$B(b) = 4[\ \sqrt{b/d} + \sqrt{d/b}\ ]^{-2} \qquad [49]$$

is optimized by setting the beam mode confocal parameter b equal to d and

$$Z(z_0) = [\ 1 + \{2z_0/(b+d)\}^2\ ]^{-1} \qquad [50]$$

which is optimized when the plane of the electrode axes is located at the beam-waist.

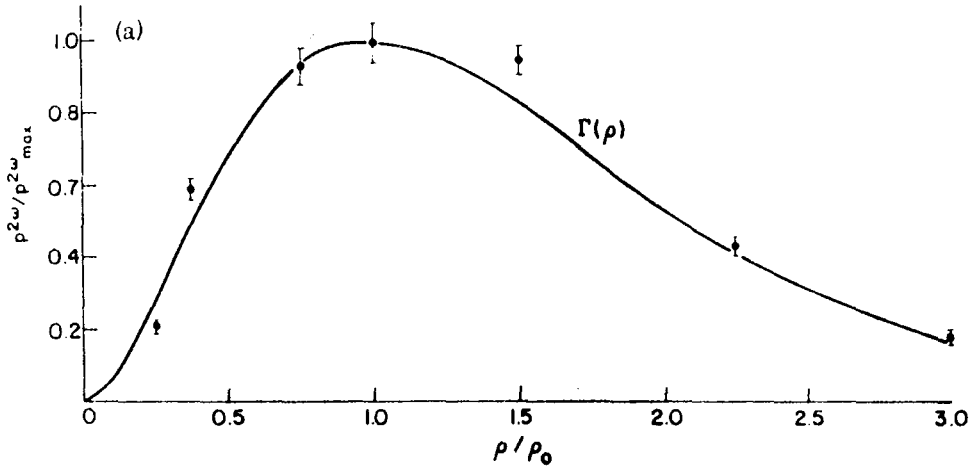

Fig.8.a. The fit between the theoretical curve $\Gamma(\rho)$, eq. [48], and experimental values, for nitrogen, is seen to be good.

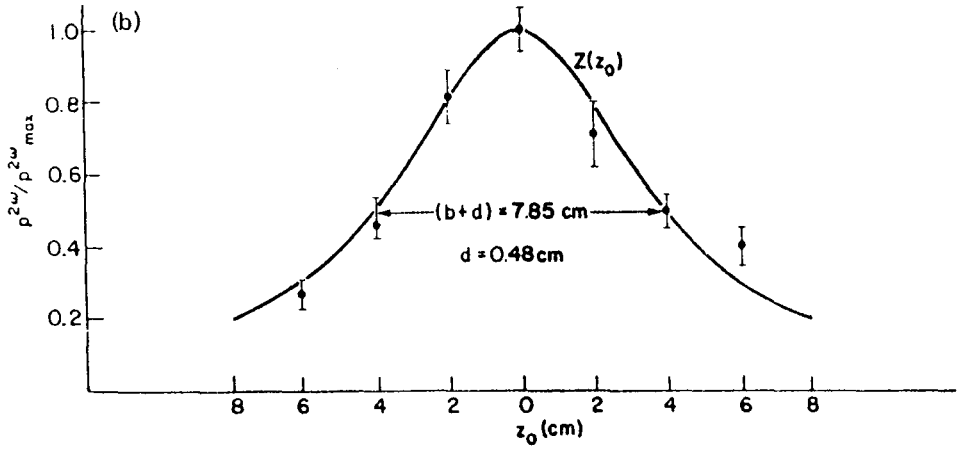

Fig.8.b. The variation of optical harmonic power, in this case air, is shown as the electrodes are moved along the optical beam.

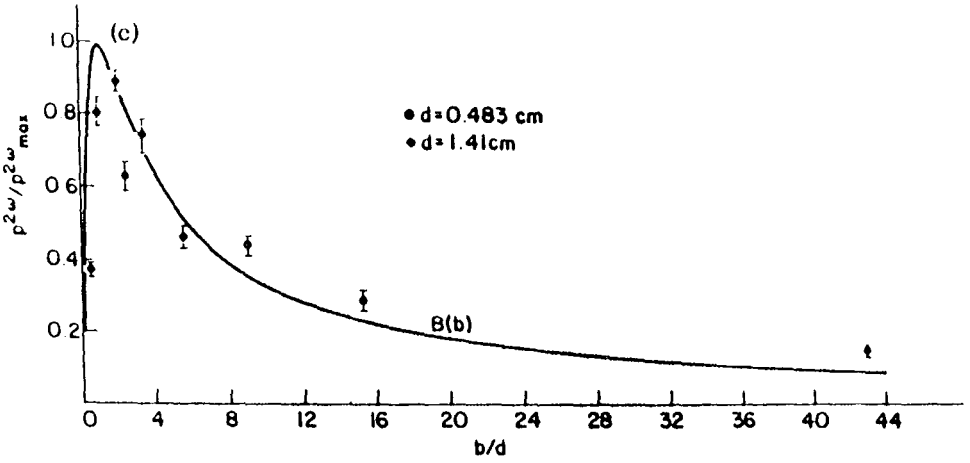

Fig.8.c. In this case equation [49] has been fitted to experimental data.

All the figures above normalize $P^{2\omega}$ to unity at the maximum. They give a hint of the parameters and in what extent they affect the power of SHG. If we assume that $z=z_0$, equation [46] reduces to

$$E_y^0(z) = 2V/\{d \cdot \cosh^{-1}(1/2a)\} \qquad [51]$$

which can be found plotted in appendix II, for different values of 1, the distance between the electrode axes. The effect of $z \neq z_0$ is also plotted and the graphs can also be found in appendix II.

CHAPTER 3: OTHER POSSIBLE METHODS

Several alternative methods to measure electric fields in gases are known. Some of these possible electro-optical phenomena in gas phase will be considered below, of which two have previously been investigated at LTH, namely

* changes in the refractive index (section 3.1)

* local modulation of the dielectric constant (section 3.6)

3.1. Changes in the refractive index due to an electric field

When a medium is subjected to an electric field a hydrostatic pressure comes up in the medium due to an attraction of polarizable molecules to regions of high field strength. The effect can be understood from the following one-dimensional case. In an inhomogenous electric field, E(x), a dipole is influenced by the force

$$F_x = \mu \, \partial E/\partial x \qquad [1]$$

where μ is the dipole moment. This force tends to pull the dipole to the area with the highest field strength. Using a real medium forces us to substitute μ with the sum of a number of the dipole moments and thus get P, i.e. the dipole moment per unit volume. P is given by

$$P = D-\varepsilon_0 E = \varepsilon_r \varepsilon_0 E-\varepsilon_0 E = (\varepsilon_r-1)\varepsilon_0 E \qquad [2]$$

The force F_x pulls these dipoles to the field maximum and thus creates a hydrostatic pressure. Equation [1] directly yields the pressure difference Δp.

$$\Delta p = 1/2 \; PE = 1/2 \; (\varepsilon_r-1)\varepsilon_0 E^2 \qquad [3]$$

where ε_r is the lowfrequency dielectric constant.

Now, let us consider a case where the medium is a gas in which we have an increase in pressure, Δp, which results in an increased density since the gas is compressible. Assume, in the name of simplicity, that the gas is ideal, one then gets the relative density increase $\Delta\rho/\rho$

$$\Delta\rho/\rho = \Delta p/p \qquad [4]$$

The polarizability (ε_r-1) of the medium is proportional to gas density, i.e., the number of molecules per unit volume, which leads to an increase in (ε_r-1) when the gas is compressed. Thus,

$$\Delta(\varepsilon_r-1)/(\varepsilon_r-1) = \Delta\rho/\rho = \Delta p/p \qquad [5]$$

This relation holds for all frequencies, both at low frequencies and at optical frequencies. The increase in pressure affects the refractive index in the visible wavelength region and one gets,

$$\Delta(\varepsilon_r^{opt}-1)/(\varepsilon_r^{opt}-1) = \Delta p/p \qquad [6]$$

where $\varepsilon_r-1 \approx 1.4\cdot10^{-3}$ at normal pressure ($p=10^5$ N/m^2). In the visible region where the optical absorption is negligible ($k\approx0$) the refractive index is given from

$$\varepsilon_r^{opt}-1 = n^2-k^2-1 \approx n^2-1 \qquad [7]$$

Differentiating gives

$$\Delta\varepsilon_r^{opt} = 2n\Delta n \qquad [8]$$

The change Δn, due to the pressure increase Δp according to eq. [6] turns out to be

$$2n\Delta n/(n^2-1) = \Delta p/p = (\varepsilon_r-1)\varepsilon_0 E^2/2P \qquad [9]$$

As $n\approx1$ we get

$$\Delta n = (n^2-1)(\varepsilon_r-1)\varepsilon_0 E^2/4P$$

where (ε_r-1) is the low frequency (below microwave frequency) polarizability. Reference [13] gives the following values for SF_6 at normal pressure

$$\varepsilon_r-1 = 2.1\cdot10^{-2}$$

$$n^2-1 \approx 1.4\cdot10^{-3}$$

To measure the small change in the refractive index we let a beam of light with wavelength $\lambda=0.5\mu$m (visible light) travel a distance $d=1$m and note the phaseshift $\Delta\phi$ due to the change in Δn

$$\Delta\phi = 2\pi d\Delta n/\lambda = 2\pi d(n^2-1)(\varepsilon_r-1)\varepsilon_0 E^2/4P\lambda = 0.92\cdot10^{-15}E^2 \quad [V/m]$$

or

$$\Delta\phi = 0.92 \cdot 10^{-3} E^2 \quad [kV/mm]$$

in SF_6 at normal pressure. At a pressure of 6 bar $\Delta\phi$ turns out to be approximately 5 times larger. To be able to measure a phase-difference of this magnitude one will probably need a stable interferometer setting, fieldmodulation and phase sensitive detection.

3.2. Stark-effect; electronic states

The possibility of directly using the Stark-effect splitting of electronic states as a way of measuring electric fields in a gaseous medium is, due to several factors, considerably more favourable than in solid materials.

At normal pressure, gases have about three orders of magnitude lower density than liquids. This implies a correspondingly reduced broadening of the atomic energy levels. Stark-separation could, in favourable cases, thus be comparable to or even larger than the natural linewidth. Contradictory to transformer oil, gases do not possess a strong, continuous absorption in the ultra-violet region of the spectrum. Thus, it is in principle possible to excite suitable levels in,e.g., atomic hydrogen. When doing field measurements in SF_6 one can study either the Stark-effect in SF_6 or in a mixture of SF_6 and a gas with a suitable Stark-spectrum.

3.3. Stark-effect; rotational states

Molecules with a permanent dipole moment tends to orient themselves along the electric lines of flux, if one applies an electric field. The energy contribution from dipole orientation is given by

$$\Delta W = -pE \cos\alpha \qquad [10]$$

where p is the dipole moment, E is the electric field and α is the angle between p and E. Even if this energy is substantially less than the thermionic average energy, kT, the molecule is not oriented, but the rotational motion is affected and one gets an energy separation from its rotational energy. If the molecule has a permanent dipole moment the Stark-effect will be linear in E (the electric field), while if the molecule only has an induced dipole moment the Stark-effect will instead have a quadratic dependence in E and thus be considerably weaker.

In a centro-symmetric gas, an electric field can induce an electric dipole moment proportional to E, and give rise to an energy of interaction proportional to E^2. In second order perturbation theory the energy shift of the unperturbed state $|\gamma JM_J\rangle$ is

$$\Delta W = e^2E^2 \sum_{\gamma'J'} |\langle \gamma JM_J|z|\gamma'J'M_J\rangle|^2 \; / \; (W_{\gamma J}-W_{\gamma'J'})$$

where the direction of the electric field $\underline{E}$ defines the z-direction. This is the quadratic Stark-effect, where it is necessary that the states $|\gamma JM_J\rangle$ and $|\gamma'J'M_J\rangle$ have opposite parity.

Experimentally, the effect can be observed through direct studies of the rotation bands in the microwave region. This implies experimental problems in general, and in particular when trying to achieve 3-dimensional resolution. Indirectly one can study the rotational levels through superposition of rotation-vibration bands in the infrared region, which removes some of the experimental problems.

SF_6 has no permanent dipole moment, thus only the quadratic effect can be expected. Possibly one could add molecules, with a permanent dipole moment, to the gas and let them act as flux indicators. If one uses high pressure, 1 bar, there will be broadening effects that tend to hide the Stark-separation of the energy levels.

3.4. Polarized fluorescence

To get an electric fieldinduced change of the polarization in a fluorescent molecule in the gas, a static orientation of the molecule is necessary. This requires a molecule with a large permanent dipole moment. If the addition of such a molecule is electrically acceptable the method could prove to be useful when measuring electric field-strengths in a gas.

3.5. Infrared absorption induced by an electric field

The infrared spectra of SF_6 consists of a few absorption peaks, whose existence are predicted by the symmetry of the molecule (octahedral symmetry). A few more vibration modes have, due to symmetry reasons, forbidden infrared transitions. If the symmetry of the molecule is changed abruptly, these absorption bands would appear.

In an electric field the molecules are polarized, e.g. SF_6, which leads to a breakdown of the perfect symmetry and the previously mentioned forbidden transitions become allowed transitions, i.e., new infrared absorption bands appear. In the case of SF_6, this possibility seems rather promising.

3.6. Local modulation of the dielectric constant

A generally feasible method to measure the local electric field for an electrode configuration is obtained if one through an externally controllable effect can modulate the local dielectric constant. This can be done by changing the electromagnetic radiation, pressure, temperature etc. One way is to use a CO_2 laser, focus the beam and thus change the temperature locally. Measurements in SF_6 at low pressure have shown that the change in capacitance depends linearly on the field intensity (ref. [16]).

When using a relative modulation of the dielectric constant $\Delta\varepsilon_r/\varepsilon_r$ one gets a corresponding modulation of the voltage, $\Delta U/U$, where U is the voltage across the region where ε_r is modulated. When modulating a fraction of the volume $\Delta V/V$ in a system with approximately constant field intensity, one gets a modulation

$$\Delta U/U \approx \Delta V/V \cdot \Delta\varepsilon_r/\varepsilon_r \qquad [11]$$

In SF_6 and other gases there are good prospects of modulating ε_r with infrared radiation. SF_6 has a broad absorption band in the 10μm region, close to the strong, 10.6μm, emission line in the CO_2 laser. When exciting vibration transitions in the gas, one modulates ε_r either indirectly through heating of the gas or directly through changes in the polarizability (caused by the excitation).

Using ε_r-modulation can, in principle, give very detailed information about the field. If one uses a focused IR-beam and at the same time modulates its intensity and the position of focus it is possible to measure both the absolute value of the electric field, direction and the fieldgradient. Experiments at LTH (ref. [17]) using a mechanically chopped CO_2 laserbeam did not yield the expected accuracy, the signal-to-noise ratio was far to low and it is believed that a substantial development work is needed.

CHAPTER 4: EXPERIMENTAL

4.1. Experimental set-up

A schematic diagram of the apparatus is shown fig.9. In order to generate a green laser beam (532 nm), an infrared beam (1064 nm) from a Nd:YAGlaser was frequency doubled in a KD*P-crystal. The remaining infrared light was reflected, by two successive mirrors with dielectric coating (manufactured by Matra) into light traps. The green beam, transmitted by the mirrors, was focused between the two cylindrical electrodes in the gas cell, which is discribed in appendix II. While the apparatus was set, the gas cell contained air.

A Pellin-Broca prism was used to spatially separate the dc electric field induced second-harmonic radiation (266 nm) from the green beam. UG-5 filters were used to discriminate green light, one filter placed directly after the prism to stop the direct beam and the other in front of the monochromator entrance slit to prevent scattered green light to enter the monochromator. The monochromator was set at 266 nm and the second-harmonic radiation was detected by a photomultiplier. The signal from the photomultiplier was brought to an oscilloscope or a boxcar-integrator, in either case trigged by a PIN-diode, which was exposed to scattered light from the dielectric mirrors. In the latter case the output signal was recorded by a xy-recorder.

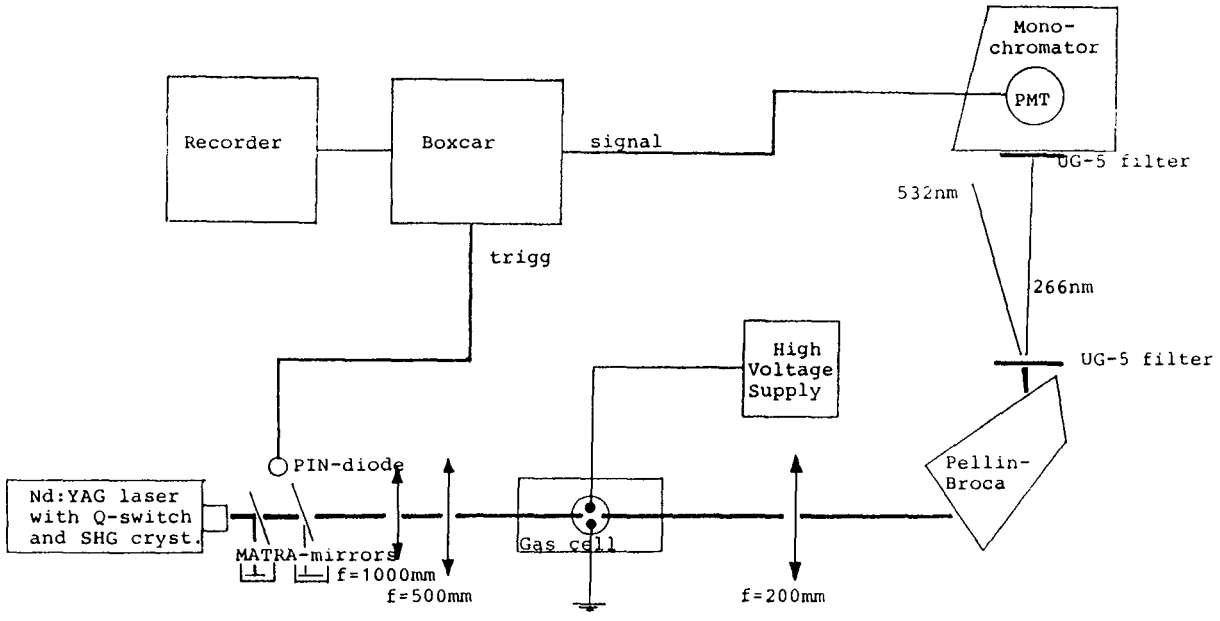

Fig.9. The experimental set-up used

To obtain maximum SHG when using cylindrical electrodes it is, as we have shown in section 2.4., essential that the laser beam focus is positioned right between the centres of the electrodes. In order to position the focus, the laserpower was increased until breakdown sparks were observed. The position of the sparks varied somewhat, but still the position of the focus could be sufficiently estimated.

Theoretically, section 2.4., the green laser beam should be vertically polarized i.e. parallel to the dc electric field to attain maximum SHG, but as the angle of incidence at the Pellin-Broca prism was near Brewster's angle, we decided to use a beam with the plane of polarization perpendicular to the dc-field, assuming that the difference in SHG would be small compared to the difference in losses in the prism. This assumption turned out to be correct.

To set the Pellin-Broca prism, in order to make the second-harmonic radiation hit the monochromator entrance slit, yet another KD^*P-crystal was used to generate a frequency quadrupled UV beam (266 nm) from the original infrared Nd:YAG laser beam. The Matra mirrors were removed and the UV light was visualized by placing a piece of paper in front of the monochromator, whereby fluorescence could be seen.

4.2. Experiments

The pressure in the gas cell was lowered to 160 mbar which was the limit for the pump used. After that the cell was filled with commercial SF_6-gas until a pressure of 1 bar was reached. This procedure was repeated three times. The Nd:YAG-laser was turned on and the signal from the photomultiplier was brought to an oscilloscope. A strong signal was discovered at 255 nm, i.e. 10 nm deviation from the expected value of 266 nm. This deviation could not be explained by experimental inaccuracy. The signal was also independent of the dc electric field.

Once more the apparatus was carefully set according to the method discribed in section 4.1.

The signal at 255 nm could no longer be seen, but when the dc-electric field was increased, a signal at 266.5 nm was discovered. This, we assumed, was due to SHG in the gas. The deviation from the expected value could be explained by an inaccuracy of the monochromator, which had been pointed out by other users. The photomultiplier was now connected to the boxcar-integrator, in single point mode. The monochromator entrance slit was 5 mm wide and the exit slit was 1 mm. The distance between the electrodes was 1.7 mm.

The following experiments were carried out:

1. SHG dependence on laserpower
2. SHG dependence on the strength of the dc-electric field
3. Change in polarization of the generating beam
4. Changes in pressure

An experiment was also carried out where the Q-switching of the laser was deteriorated and the pumping effect increased, in order to get longer pulses with retained energy. In this we gained no success.

Furthermore, we increased the distance between the electrodes but could then not detect any signal. Neither could we detect any signal when using spherical or flat electrodes.

4.3. Experimental results

In this section the results will be presented and compared with the accepted theory and the approximations made in section 2.4. Note that, these approximations are only valid for cylindrical electrodes. If nothing else is stated, we will assume that the laser beam focus is positioned at the origin,i.e., $z=z_0$. A few of the most important formulae from sec. 2.4. will be given again

$$E_y^0(z) = \{2V/[d\cdot\cosh^{-1}(1/2a)]\}\cdot\{1/1+[2(z-z_0)/d]^2\} \qquad [46]$$

$$P^{2\omega}=(P^{\omega})^2(E_y^0(z_0))^2(36\pi^4L^2\omega^3/e^2c^4)[\chi/\Delta k_0]\ 1/d\ \Gamma(\rho)B(b)Z(z_0) \qquad [47]$$

Note that, the second part of eq. [46] equals one when $z=z_0$ and that the second harmonic power has a quadratic dependence on the electric field strength and thus also on the applied voltage,V. The two parts of eq. [46] have been plotted seperately, and can be found in appendix II.

The results are discussed and evaluated in chapter five.

4.3.1. The SHG signal's dependence on laserpower

According to eq. [47] the SHG signal, $P^{2\omega}$, could be expected to be quadraticly dependent on the laser power, P^{ω}. In figure [10] we can see a typical output signal for a few different values of laser power.

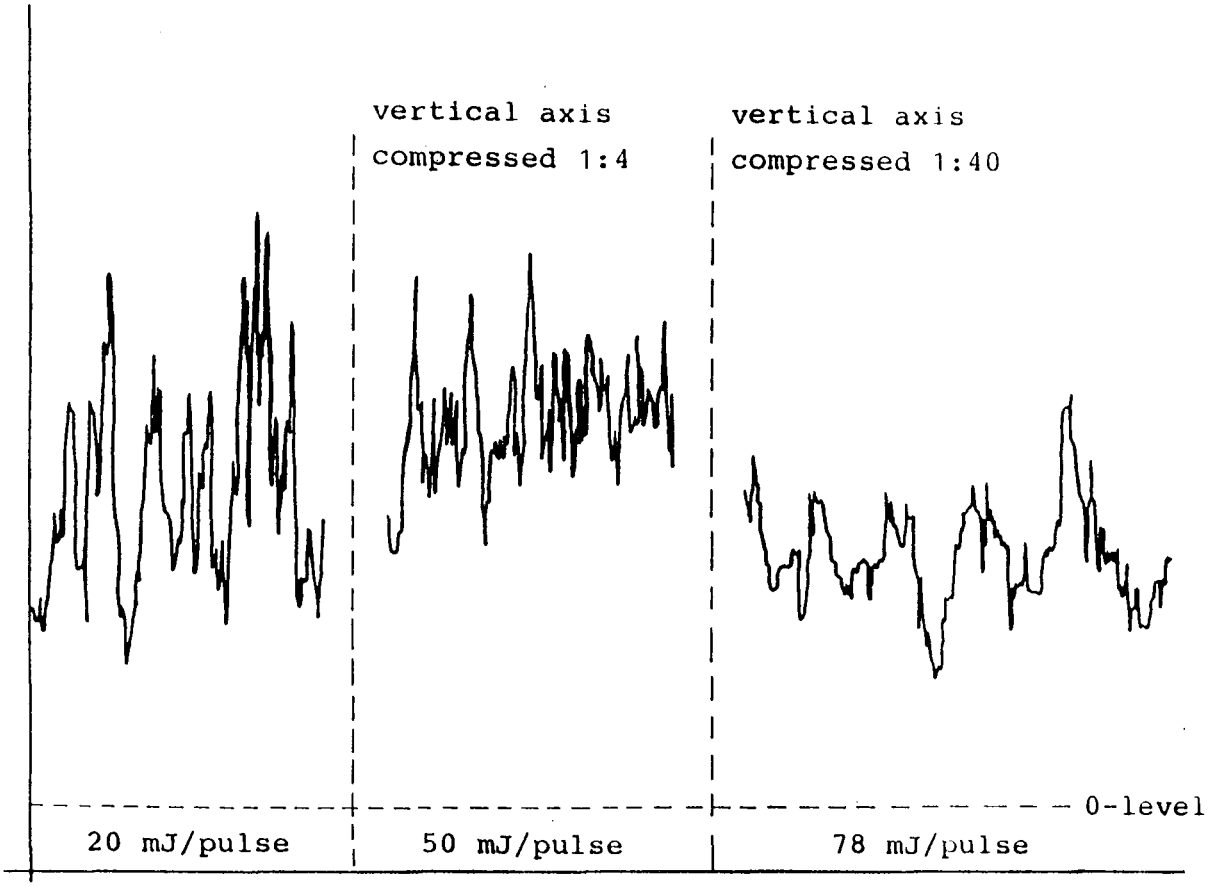

Fig.10. A typical output signal, recorded on an xy-recorder, for various values of laser power.

The average signal level was measured and fitted to the following two curves, using a least-squares approximation

1. $y = A + Bx$
2. $y = A + Bx^2$

The error was estimated from the fluctuations in the signal,i.e., we wanted 90% of the signal to be within the error limit, see fig. [11].

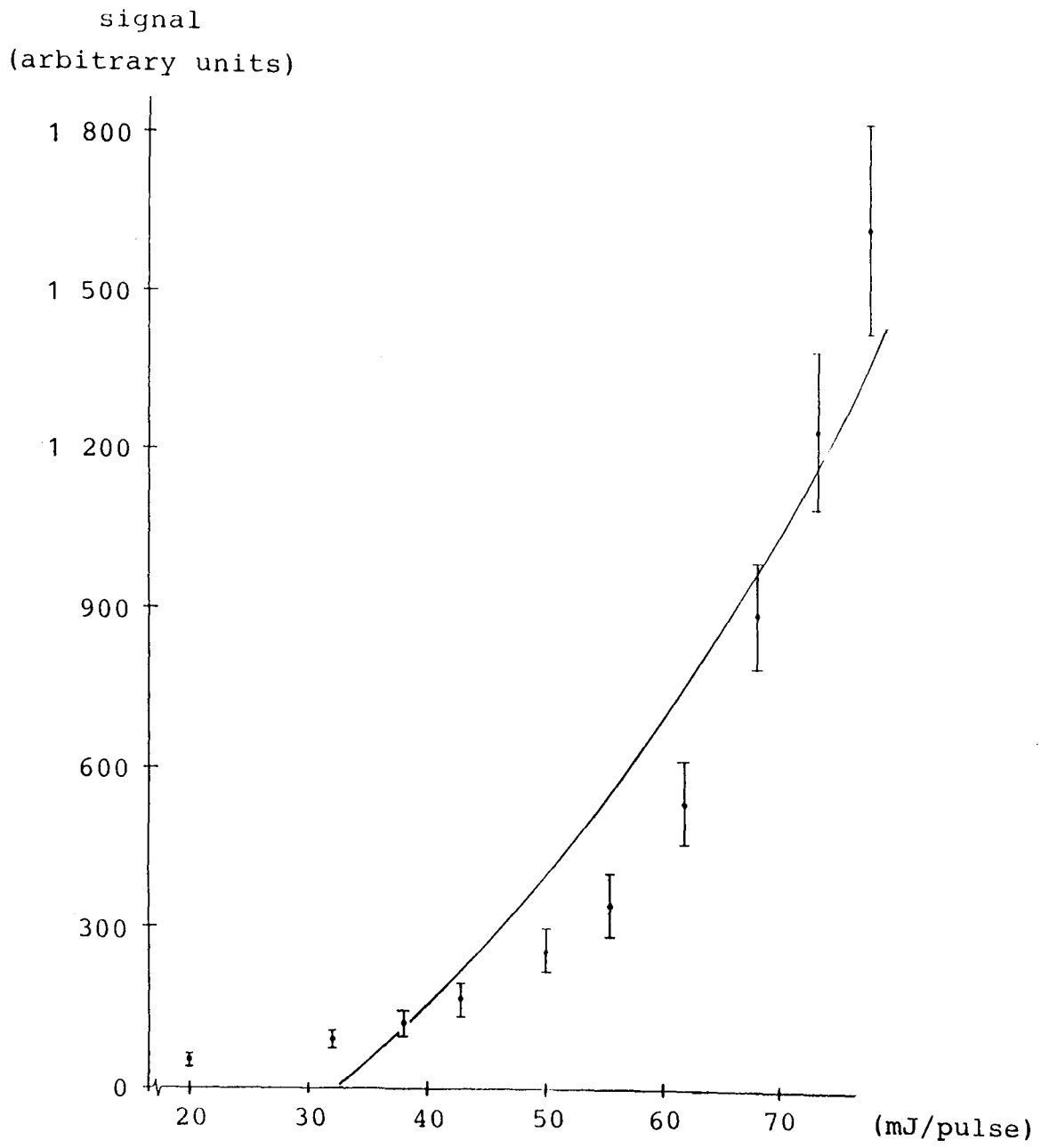

Fig.11. A quadratic curve, $y = -283 + 0.27x^2$, was fitted to the aquired data.

When fitting the data to the curves, the correlation coefficient, R, was determined as well.

1. R= 0.03 when using the linear fit
2. R= 0.95 when using the quadratic fit

4.3.2. The SHG signal's dependence on the dc electric field

When studying eq. [46] and [47] we find that the SHG signal, $P^{2\omega}$ ought to have a quadratic dependence on the applied dc-voltage. In figure [12] we can see the signal obtained with the boxcar-integrator in single-point mode while figure [13] shows the signal when sweeping the monochromator setting from 255nm to 275nm and using a boxcar window of 15ns and a moderat time constant.

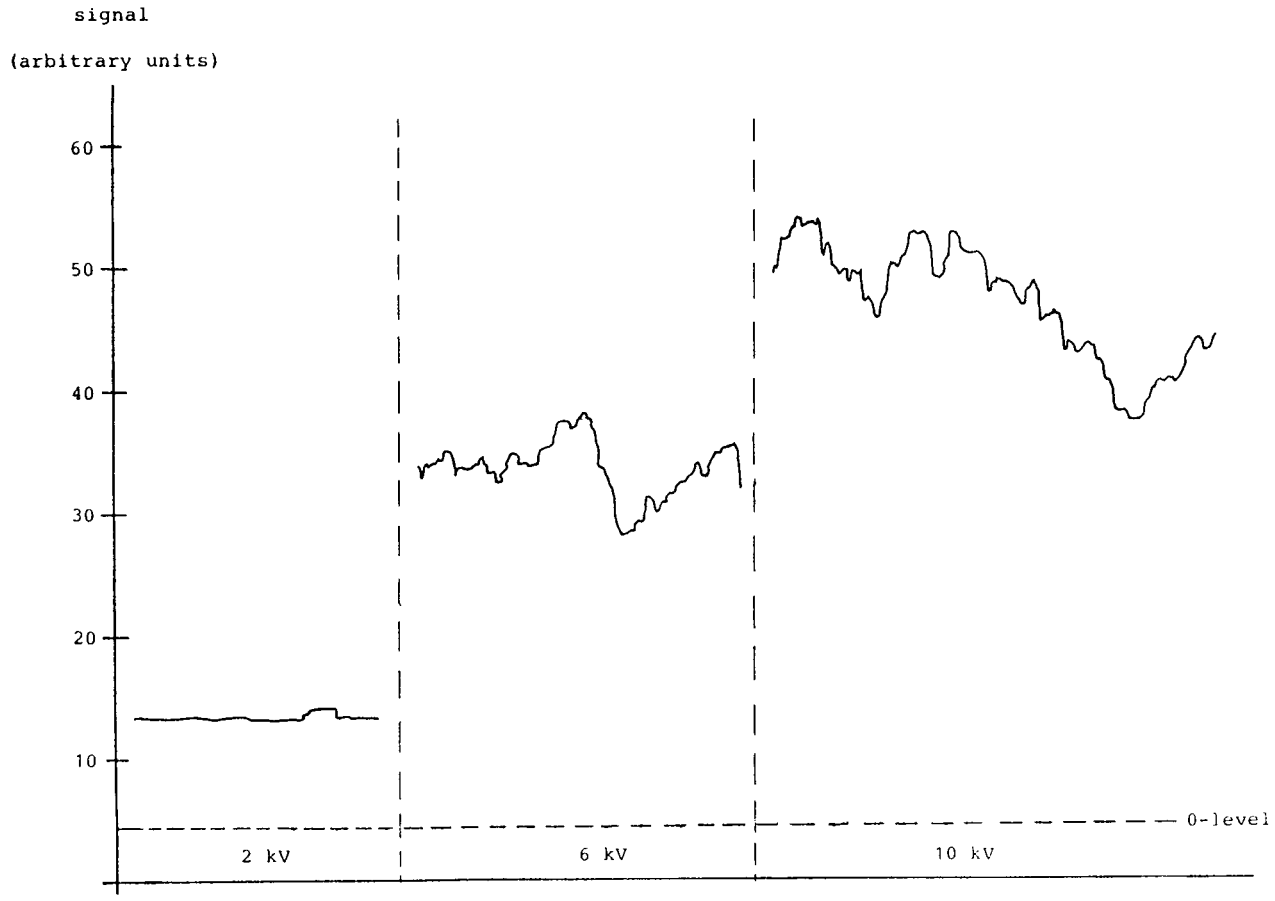

Fig.12. The signal obtained from the boxcar-integrator when using single-point mode, for various applied dc-voltages.

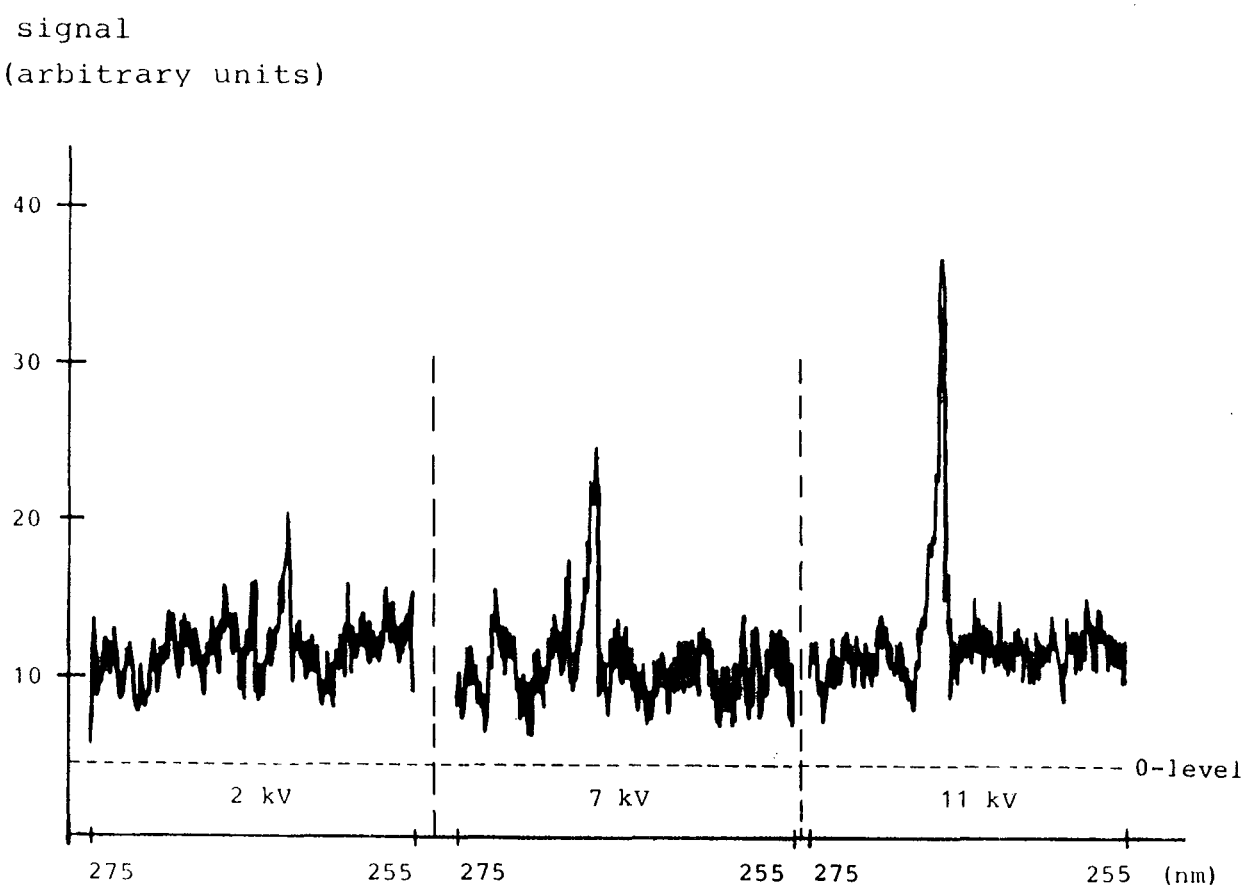

Fig.13. The signal obtained from the boxcar when sweeping the monochromator setting from 255nm to 275nm for, a few different dc-voltages.

Using the graphs in appendix II one easily finds that when V, the applied dc-voltage, varies between 0 kV and 12 kV, the electric field strength varies between 0 kV/mm and 6.9 kV/mm.

The data was fitted to the same two curve types as in section 4.3.1., i.e., to a linear and a quadratic expression, using the least-squares method. When estimating the error, the same criteria was used as in section 4.3.1. The correlation coefficient was evaluated in both cases.

1. $y = 1.58 + 4.33x$ with $R = 0.96$
2. $y = 8.57 + 0.37x^2$ with $R = 0.99$

The data has been plotted in figure [14] along with the quadratic equation given above, which is the best fit to the data.

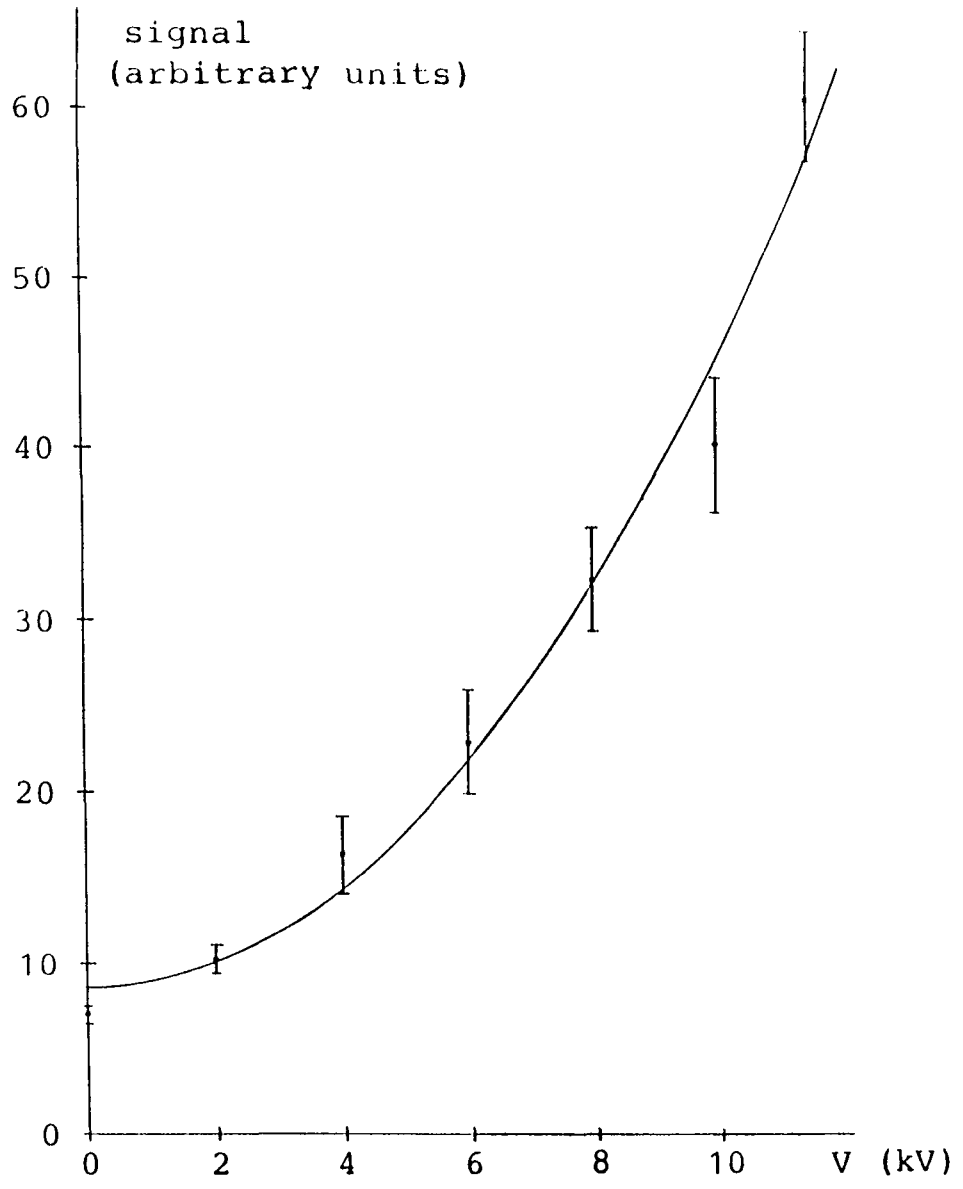

Fig.14. A quadratic expresion has been fitted to the aquired data. In this case the correlation coefficient, R, equals 0.99.

4.3.3. Change in polarization of the generating beam

According to section 2.4. one can assume the SHG signal to be three times stronger when having a dc electric field parallel to the polarization of the laser beam than when the dc electric field is perpendicular to the polarization of the laser beam. To find out whether this was true for the experimental set-up, as a whole, including all optical components, an experiment was carried out.

We applied 9 kV across the cylindrical electrodes and used a laser power of approximately 5 MW (peak value).

1. When the laser beam was polarized parallel to the dc electric field we got a SHG corresponding to 27 units on the xy-recorder.

2. When the polarization was changed to be perpendicular to the dc electric field the aquired signal increased to 40 units.

The quotient between the result in 1. and 2. turns out to be 0.7 instead of the expected 3.0, which is approximately a factor 4 short of the expected result.

4.3.4. Changes in pressure

The effect of lowering the pressure was studied, but did not give any information about the extent in which SHG is affected. According to eq. [48] and figure 8.a. we have a slow decrease in SHG when the relative density of SF_6 decreases and this, in turn, induces breakthroughs. Thus, in our case, the experiment did not give any relevant information.

CHAPTER 5: EVALUATION OF EXPERIMENTS

Our intentions are to compare the experimental results with the theory given in section 2.4. No attempt is made to produce empirical formulae based on the recorded data. At this stage of developing a measuring method, we do not find it relevant to present a mathematical relation based on the experimental data.

5.1. Evaluation of experimental results

During the experiments, discharges between the electrodes appeared randomly, each resulting in a peak which slowly declined to the initial signal level. This possible error in the signal level was reduced by disregarding the information recorded during and shortly after discharge peaks. On the other hand, the effects of a discharge on the properties of SF_6 were difficult to estimate, although a deterioration of the insulating properties can be expected, and thus introducing an error in our measurements.

We assume that possible temperature gradients in the gas do not substantially change the refractive index of SF_6 and thus causing a change in the direction of the second harmonic. By extrapolating in fig.6. and using eq. [12], one finds the coherence length to be approximately 5 mm. The coherence length does not impose any restrictions on SHG, because of a small laser focus and a rapidly decreasing electric field (when $z \neq z_0$).

5.1.1. The SHG signal's dependence on laser power

According to the theory given in section 2.4. the SHG signal should depend quadraticly on laser power. As can be seen in figure 12, the least-squares fit does not suggest a dependence in conformity with theory. It is also of value, when designing a measuring method, to be able to determine the laser output power needed to get a sufficiently strong SHG signal, when applying a specific dc-voltage. Several sources of error are evident:

* The radiated energy is not constant between successive pulses.

* Within each pulse the radiated power is unevenly distributed. When measuring the laser output power the result obtained is an average value. This value does not give sufficient

information to calculate the power of the second harmonic, due to the SHG's quadratic dependence on laser power.

* The mode structure obtained from the laser was poor, due to a partly malfunctioning Q-switch. This sets a limit to the the minimum obtainable beam waist diameter and causes a less distinct focus.

5.1.2. The SHG signal's dependence on the dc electric field

The experimental data was fitted to a quadratic curve, see figure 14, with good correlation (R=0.99). The signal obtained when no dc-voltage was applied between the electrodes deviated somewhat from zero, which is the theoretical value. The origin of the constant signal is unknown, but we do not doubt that it can be substantially reduced when using an improved experimental set-up. We base this argument on the fact that we have already managed to reduce it by trimming the experimental set-up used. Part of this constant signal may have been generated in the fused silica used in prism, lenses and end-gable windows.

Errors and deviations from theory can also be caused by:

* the electron flow between the electrodes. This is a known phenomenon in breaker applications when using HVDC-equipment, and as we have used relatively strong electric fields it is not unlikely that it occurs here as well. This probably causes a reduction of the effective potential difference between the electrodes.

* the rippled dc-voltage used. We had no access to a perfect dc-voltage, instead a full-wave rectification of the available triphase ac-voltage was made. This resulted in a dc-level with superpositioned ripple, which might disturb measurements made on weak electric fields, i.e., when low voltages are applied between the electrodes.

5.1.3. Change in polarization of the generating beam

Theoretically, the generating laser beam should be polarized parallel to the dc electric field, thus generating a second harmonic with the same polarization. The discrepancy between theory and experiments can be explained by the unfavourable angle of incidence at the Pellin-Broca prism, i.e., close to Brewster's angle. Thus, a stronger signal was obtained when using a laser beam polarized perpendicularly to the dc electric field.

Choosing an experimental set-up, in which a laser beam polarized parallel to the dc electric field is favoured, a stronger signal can be expected. One way of acheiving this is by rotating the electrodes 90°, unfortunately this was not possible in our set-up.

5.1.4. Changes in pressure

According to reference [11], the optimal pressure for SHG in SF_6 is 1.09 bar at 0° C. When studying equation [48] one finds that the optimum is relatively flat, hence the pressure is not critical. An attempt to decrease the pressure and measure the SHG signal, resulted in a rapid increase of discharges, thus making the recorded signals impossible to evaluate.

5.2. Improvements of the experimental set-up

In order to reduce some of the disadvantages pointed out above, we suggest the following, improved experimental set-up.

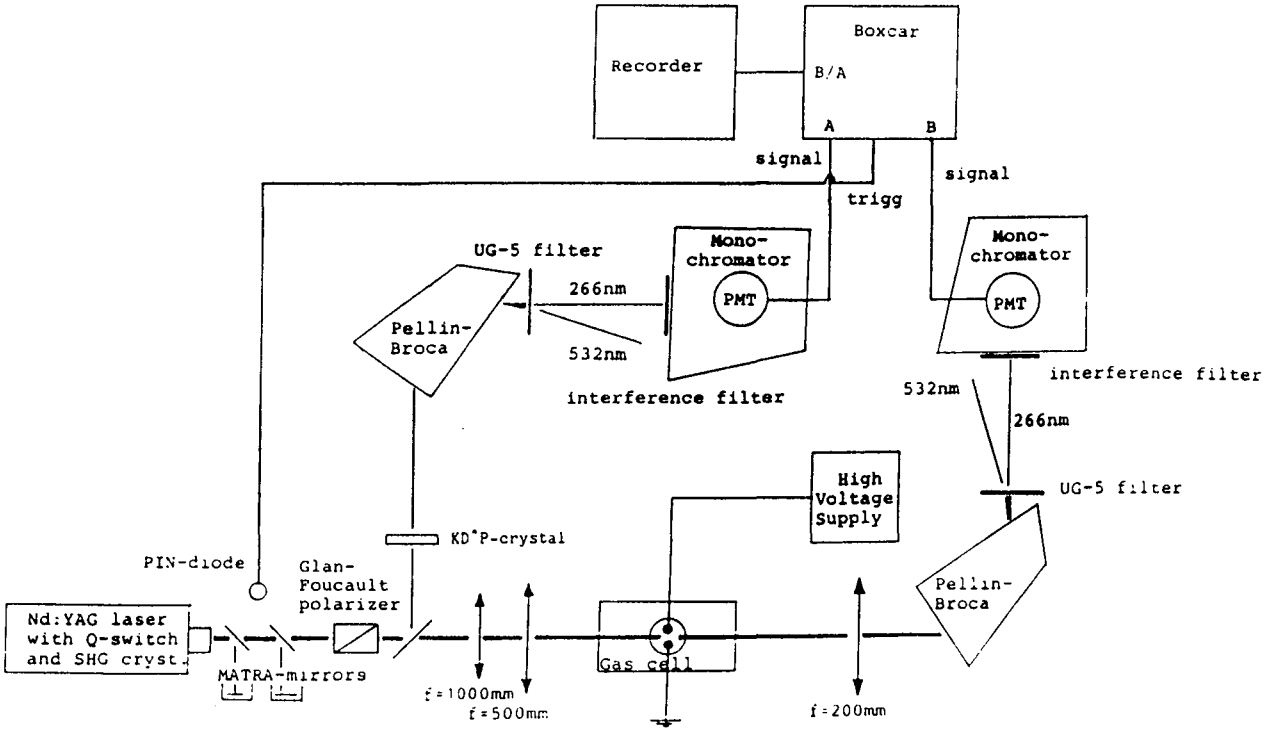

Fig.15. Suggested improved experimental set-up.

* A Glan-Foucault polarizer is inserted into the laser beam in order to guarantee uniform polarization in a specified direction.

* A beam-splitter is used to deflect a reference beam to a KD^*P-crystal. The frequency doubled signal is then compared to the second harmonic generated in the gas cell. Using this technique, fluctuations between successive pulses of the generating beam cancel out. This implies a less fluctuating second harmonic.

* One of the UG-5 filters is exchanged for a suitable interference filter.

With these improvements, we believe that a functionable measuring method can be developed and used in the laboratory.

SUMMARY

The assumption usually made in classical optics, i.e. that the induced dielectric polarization of a medium is linearly related to the applied electric field, is not valid when using high-power lasers. Instead one finds that the nonlinear part becomes non-negligible, which results in the generation of second harmonic. In centro-symmetric gases the susceptibility of the second order is zero, due to the symmetry, but if a dc electric field is applied the symmetry is broken up and SHG is possible.

This implies a way of measuring the electric field strength in a centro-symmetric gas (e.g. SF_6) without having to use a probe. Possibly one could even achieve a 3-dimensional resolution of the field gradient. To test these assumptions, a measurement cell was constructed and fitted with cylindrical electrodes connected to a high voltage supply (0-12 kV).

When investigating the power of the generated second harmonic and its dependence on the used laser power, we got a mediocre correlation with theory, i.e., a poor fit to a quadratic curve. This divergence from theory, most likely depends on the very poor laser mode obtained from the Nd:YAG laser used.

The SHG signal was found to depend on the electric field quadraticly, in accordance with theory. The field dependent signal was superimposed on a constant signal, which may have been generated in the fused silica used in various optical components.

An improved experimental set-up can be achieved by using a reference signal of the same frequency. The second harmonic generated in the gas cell is compared to this signal, thus yielding a less fluctuating, normalized signal.

We believe a functionable measuring method can be developed using the improved experimental set-up.

REFERENCES

I. SHG

i) Books

[1] Baldwin,G.C. — An Introduction to Nonlinear Optics; Plenum Press, 1969, New York, USA

[2] Bloembergen,N. — Nonlinear Optics; W.A. Benjamin Inc., 4th printing, 1982, Reading, Mass., USA

[3] Borgström,S. — Laserfysik; Sigmatryck, LTH, 1985, Lund

[4] Svanberg,S. — Atom- och molekylspektroskopi; Sigmatryck, LTH, 1985, Lund

[5] Svelto,O. — Principles of Lasers; Plenum Press, 2nd edition, 1982, New York, USA

ii) Articles and technical reports

[6] Bigio,I.J./Ward,J.F. — Physics Review A; vol. 9, nº 1, page 35, 1974

[7] Bigio,I.J./Ward,J.F. — Physics Review A; vol. 11, nº 1, page 60, 1975

[8] Finn,R.S./Ward,J.F. — Physics Review Letters; vol. 26, nº 6, page 285, 1971

[9] Hjortsberg,A — Teknisk rapport TR KYJU 82-064; 820809, ASEA RESEARCH

[10] Hörnfeldt,S/Montan,S — Rapport angående försök med frekvensfördubbling i SF_6; 17-25/2 1983, LTH and ASEA RESEARCH

[11] Ward,J.F./Miller,C.K. — Physical Review A; vol. 19, nº 2, page 826, 1979

[12] Siemens — Technical Report on SF_6 and Its Properties

II. Refractive index change

[13] ASEA — Technical Report RM KYJU 83-095; ASEA

III. Stark-effect, electronic and rotational states

[14] Woodgate, G.K. — Elementary Atomic Structure; Oxford Science Publications, 2nd edition, Oxford, 1983

[15] Bischel,W.K. et.al. — Physics Review Letters; vol. 34, no 6, page 300, 1975

IV. Polarized fluorescence

see reference [9]

V. Infrared absorption induced by an electric field

see reference [9]

VI. Local modulation of the dielectric constant

[16] Bazarov,E.N. et.al. — Sovjet Journal of Quantum Electron.; no 8, page 618, May 1978

[17] Borgström,S./ASEA — Technical Report RR KYJU 83-063; June 1983, ASEA/LTH

APPENDIX I.

Equipment used

Laser: Nd:YAG from Quanta Ray. It was equipped with a Q-switch (Pockel's cell) and crystals for second, third and fourth harmonic generation.

SHG 532nm
THG 355nm Quanta Ray: model HG2
FHG 266nm serial no 587

Laser data:

λ (nm)	pulse width (ns)	max pulse energy (mJ) amplifier/oscill. only
1064	8 - 9	800/300
532	6 - 7	360/150
355	5 - 6	150/60
266	4 - 5	60/20

Spatial mode: Unstable resonator, uniphase, near diffraction limited, beam diameter at least 6 mm.

Pulse repetition rate used: 10 Hz

Monochromator: Bausch & Lomb

Boxcar averager: EG&G Princeton Applied Research, USA model 162

Gated integrator: EG&G Princeton Applied Research, USA model 165

Photomultiplier: EMI 9558 serial no 23904

Photomult. house: Products for Research, USA

Power meter:	Coherent model no 201 serial no u278
XY-recorder:	BBC Goerz model Servogor 5 RE541 serial no R 692 692
Mirrors:	MATRA no 7 λ=532nm R=0.10 at 45° λ=1064nm R≈0.90 at 45°
Filter:	SCHOTT UG 5 (2mm) λ=532nm T=$0.25 \cdot 10^{-6}$ λ=266nm T=0.766
Lenses:	Three fused silica lenses; f=200mm, 500mm, 1000mm
Prism:	Pellin-Broca; fused silica
Gas cell gable:	Fused silica windows, Φ=50mm

APPENDIX II.

Graphs of the variation of the electric field strength:

1. $E_y^0(z) = 2V/\{d \cdot \cosh^{-1}(1/2a)\}$ [0-4 kV/mm]

2. $E_y^0(z) = 2V/\{d \cdot \cosh^{-1}(1/2a)\}$ [2-10 kV/mm]

3. $f(z-z_0) = 1/\{1+[2(z-z_0)/d]^2\}$

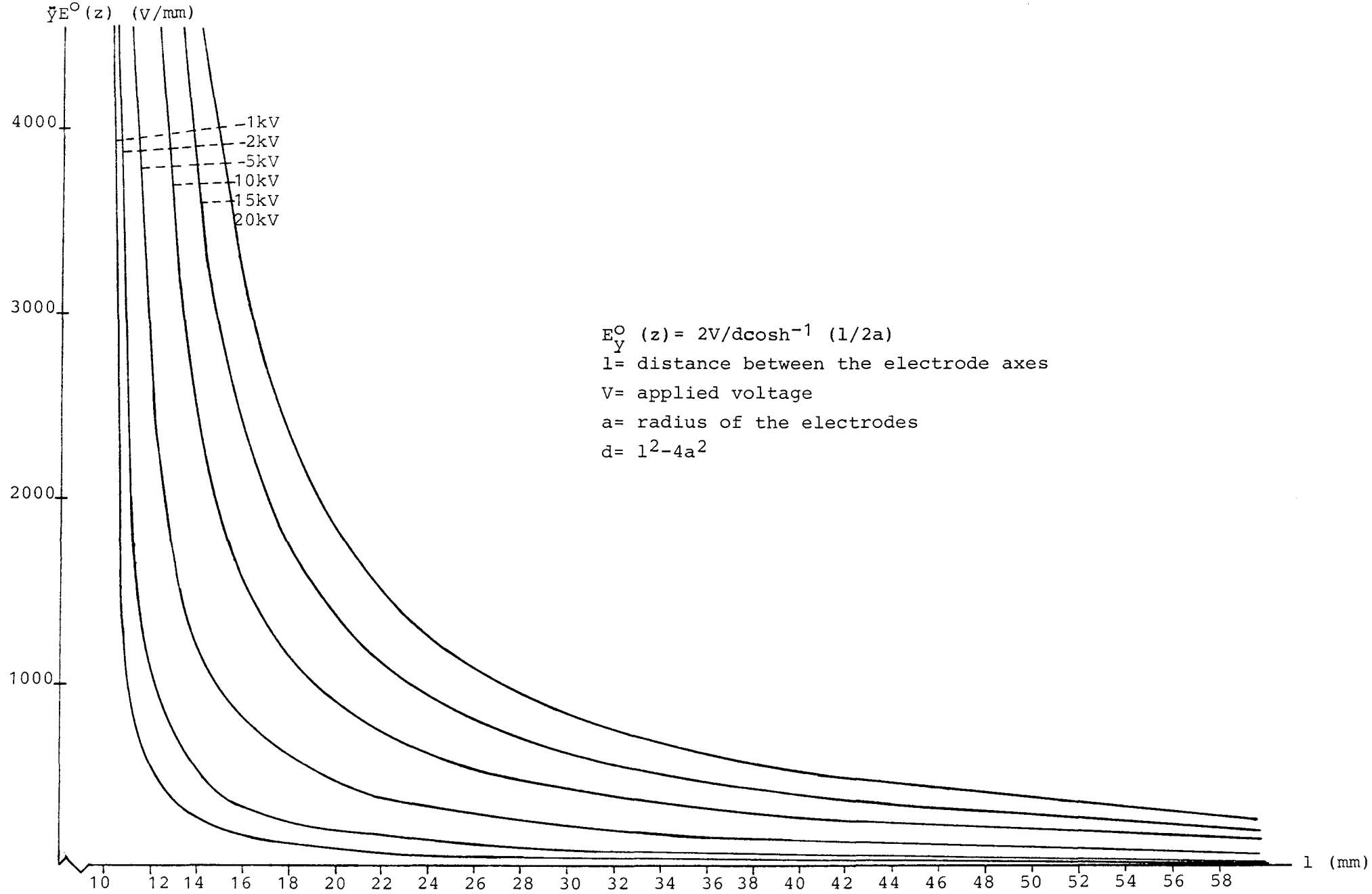
$\vec{y}E^{o}(z)$ (V/mm)
4000
3000
2000
1000
-1kV
-2kV
-5kV
-10kV
-15kV
-20kV
$E_y^o(z) = 2V/d\cosh^{-1}(l/2a)$
l= distance between the electrode axes
V= applied voltage
a= radius of the electrodes
$d = l^2-4a^2$
l (mm)
10 12 14 16 18 20 22 24 26 28 30 32 34 36 38 40 42 44 46 48 50 52 54 56 58

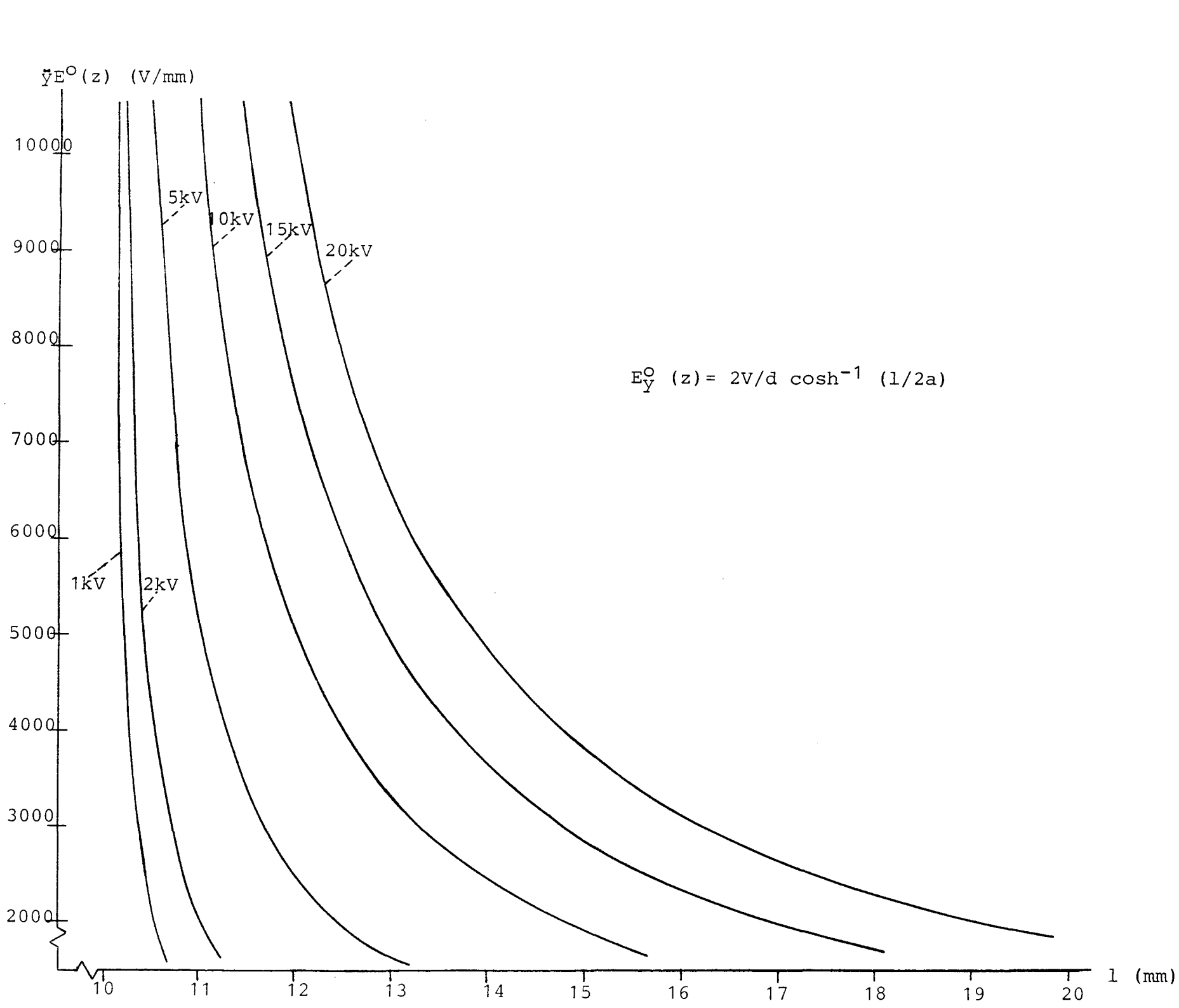
$\tilde{y}E^{o}(z)$ (V/mm)
10000
9000
8000
7000
6000
5000
4000
3000
2000
5kV
10kV
15kV
20kV
1kV
2kV
$E_y^o(z) = 2V/d \cosh^{-1}(l/2a)$
10
11
12
13
14
15
16
17
18
19
20
l (mm)

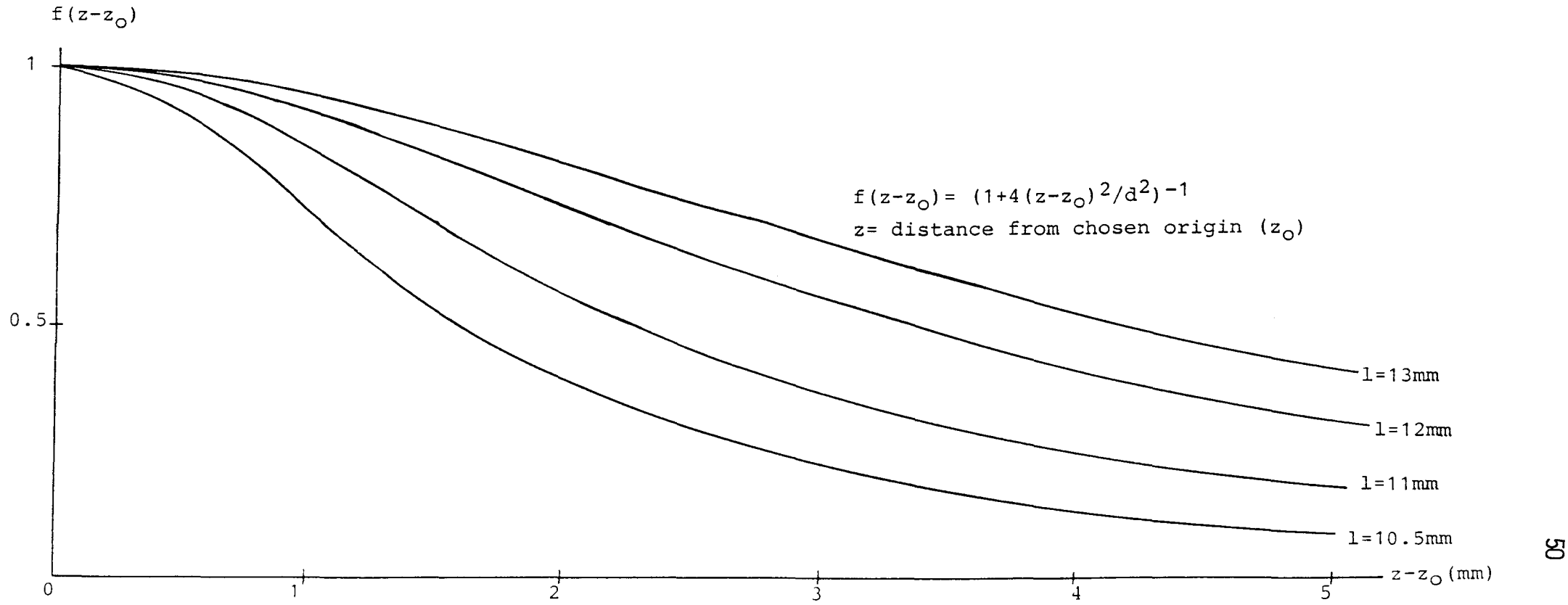
f(z-z$_o$)
1
0.5
0
1
2
3
4
5
z-z$_o$ (mm)
f(z-z$_o$) = (1+4(z-z$_o$)^2/d^2)$^{-1}$
z= distance from chosen origin (z$_o$)
l=13mm
l=12mm
l=11mm
l=10.5mm

APPENDIX III.

Curve fitting method and formulae used

We used curve fitting with least-squares approximation when fitting the curves in sections 4.3.1. and 4.3.2. The formulae used for the different fits were

A. Curve fitting to $y = A+Bx$

$$A = \{\Sigma y - B\cdot\Sigma x\}/n$$

$$B = \{n\Sigma xy - \Sigma x\cdot\Sigma y\}/\{n\Sigma x^2 - (\Sigma x)^2\}$$

$$R^2 = B\cdot\{n\Sigma xy - \Sigma x\cdot\Sigma y\}/\{n\Sigma y^2 - (\Sigma y)^2\}$$

B. Curve fitting to $y = A+Bx^2$

$$A = \{\Sigma y - B\cdot\Sigma x^2\}/n$$

$$B = \{n\Sigma x^2y - \Sigma x^2\cdot\Sigma y\}/\{n\Sigma x^4 - (\Sigma x^2)^2\}$$

$$R^2 = B\cdot\{n\Sigma x^2y - \Sigma x^2\cdot\Sigma y\}/\{n\Sigma y^2 - (\Sigma y)^2\}$$

APPENDIX IV.

Drawings of the measurement cell

Drawing no:

1. Detail no 1: assembling jig
2. Details no 2 and 3
3. Detail no 4: ground connection profile
4. Detail no 5: levelling sheet
5. Detail no 6: cylinder, Φ=160 mm
6. Detail no 7: plexiglass tube for angular assemblage
7. Detail no 8: gable-end house, Φ=160 mm
8. Detail no 9: gable-end house, Φ=80 mm
9. Detail no 10: upper electrode holder
10. Detail no 11: high tension through pass
11. Detail no 12: lower electrode holder
12. Electrodes

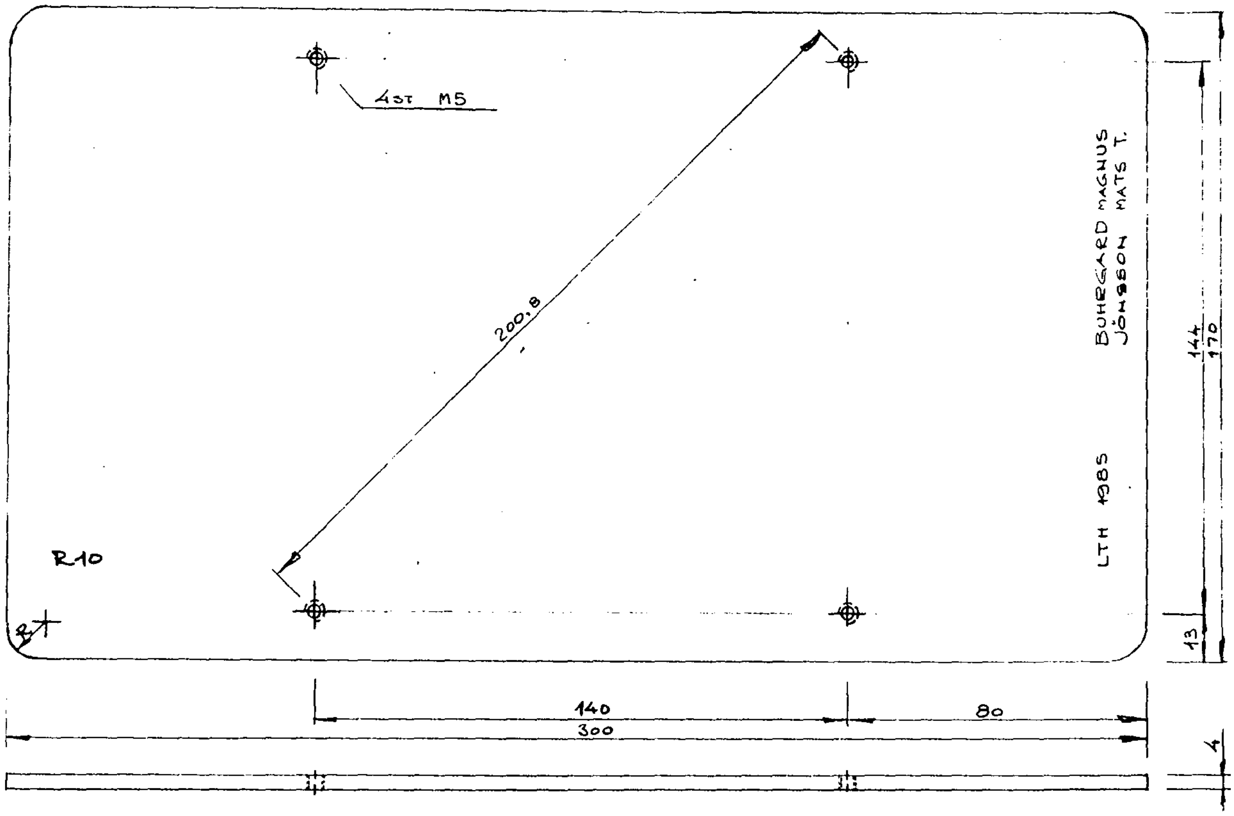

1	1	ASSEMBLING JIG	Fe-SHEET	300x170x4	YELLOW CHROMATED

1	1	MONTAGEJIGG	Fe-PLÅT	300x170x4	GULKROMATERAS
Det.-nr	Ant.	Benämning	Material	Mod.-nr Ämne Dimension	Anm.

Konstr. | Ritad: mtj | Kop. | Kontr. | Stand. | Godk. | Skala | Ersätter | Ersatt av

DETAIL Nº 1
ASSEMBLING JIG

Dat. 1985-05-25
Ritn.-nr 1

Nr	Ant.	Ändring och/eller medd.-nr	Datum	Inf.	Godk.	Nr	Ant.	Ändring och/eller medd.-nr	Datum	Inf.	Godk.

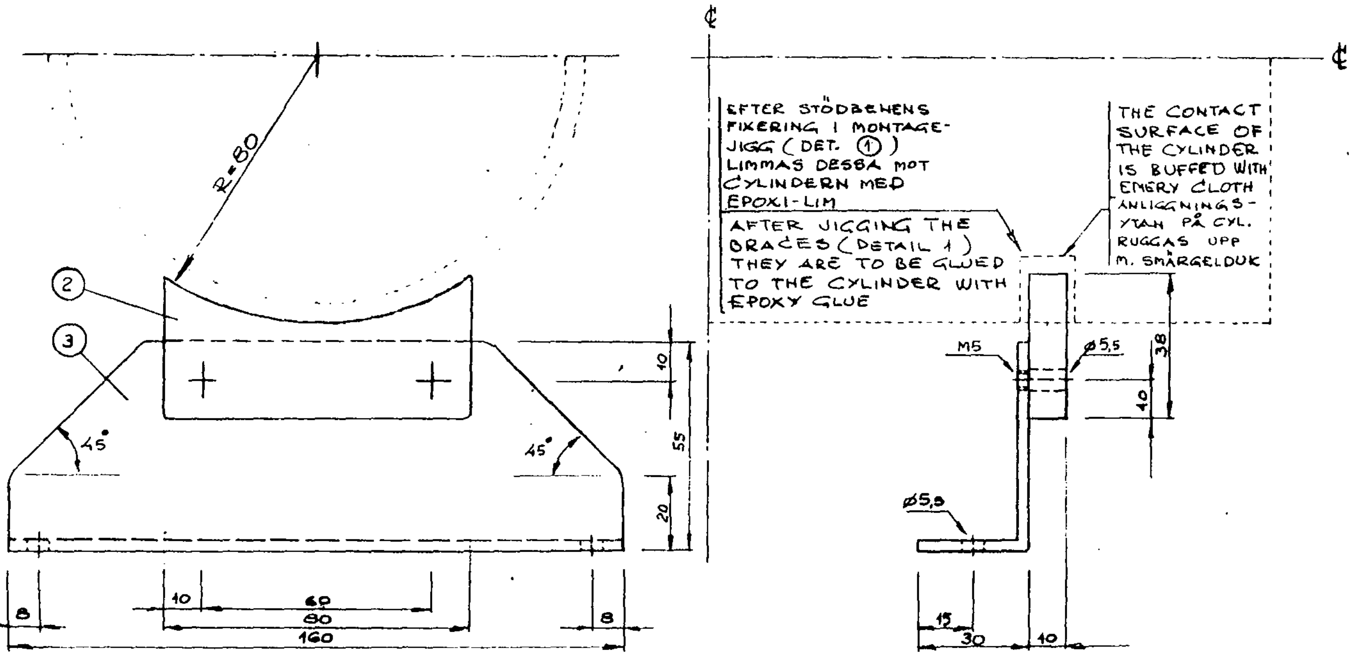

	4	WASHER BRB 5,5	STEEL		ZINCIFIED
	4	SCREW M6S 5x16	BUFO 8.8	M5 x 16	ZINCIFIED
3	2	L-PROFILE	Fe-SHEET	160x55x3	YELLOW CHROMATED
2	2	BRACE	PLEXIGLASS	38x80x10	

	4	BRICKA BRB 5,5	STÅL		ELFÖRZINKAD
	4	SKRUV M6S 5x16	BUFO 8.8	M5 x 16	ELFÖRZINKAD
3	2	L-PROFIL	Fe-PLÅT	160x55x3	GULKROMATERAS
2	2	FLÄNS (STÖDBEN)	PLEXIGLAS	38x80x10	
Det.-nr	Ant.	Benämning	Material	Mod.-nr Ämne Dimension	Anm.

Konstr. | Ritad: mtj | Kop. | Kontr. | Stand. | Godk. | Skala | Ersätter | Ersatt av

DETAILS Nº 2 o 3

Dat. 1985-05-25
Ritn.-nr 2

Nr	Ant.	Ändring och/eller medd.-nr	Datum	Inf.	Godk.	Nr	Ant.	Ändring och/eller medd.-nr	Datum	Inf.	Godk.

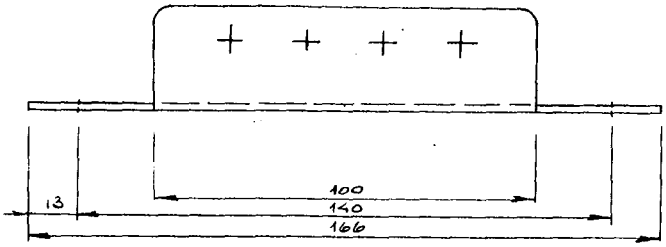

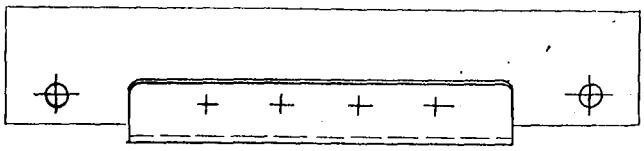

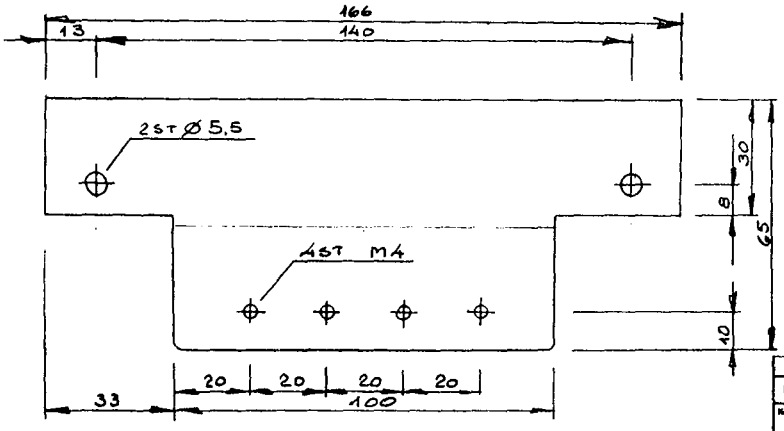

Nr	Ant.	Ändring och/eller medd.-nr	Datum	Inf.	Godk.	Nr	Ant.	Ändring och/eller medd.-nr	Datum	Inf.	Godk.

Det.-nr	Ant.	Benämning	Material	Mod.-nr Ämne Dimension	Anm.
1	1	GROUND CONNEC. PROFILE	Fe-SHEET	166×65×2	YELLOW CHROMATED
4	1	JORDANSL.-PROFIL	Fe-PLÅT	166×65×2	GULKROMATERAS

Konstr. mtj Kop. Kontr. Ritad. Godk. Skala Ersätter Ersatt av

DETAIL Nº 4

GROUND CONNEC. PROFILE

Dat. 1985-05-25

Ritn.-nr 3

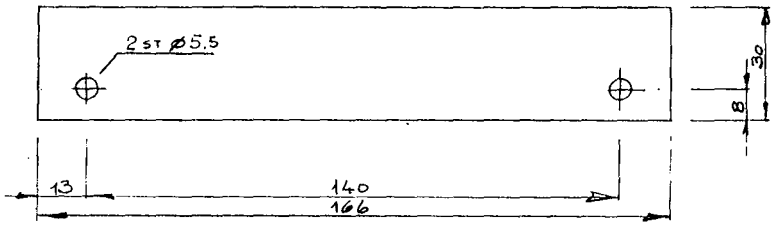

Det.-nr	Ant.	Benämning	Material	Mod.-nr Ämne Dimension	Anm.
5	1	LEVELLING SHEET	STEEL	166×30×2	YELLOW CHROMATED
5	1	NIVÅJUST.-PLÅT	STÅL	166×30×2	GULKROMATERAS

Konstr. mtj Kop. Kontr. Ritad. Godk. Skala Ersätter Ersatt av

DETAIL Nº 5

Dat. 1985-05-25

4

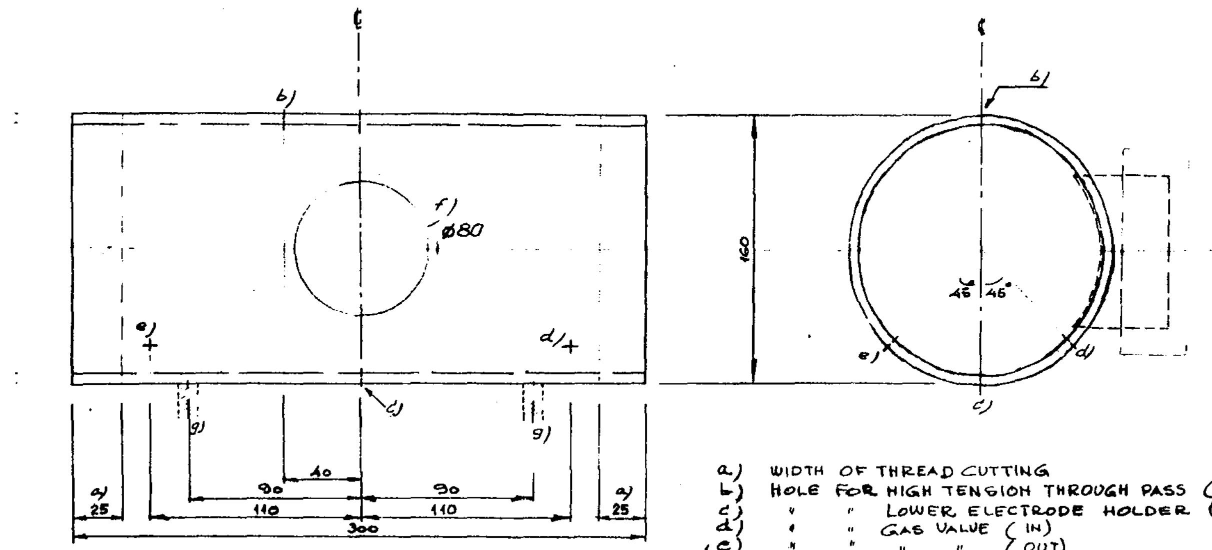

a) WIDTH OF THREAD CUTTING
b) HOLE FOR HIGH TENSION THROUGH PASS (10 kV)
c) " " LOWER ELECTRODE HOLDER (⏚)
d) " " GAS VALVE (IN)
e) " " " " (OUT)
f) " " DETAIL Nº 7
g) BRACE

a) BREDD PÅ GÄNGNING
b) HÅL FÖR HÖGSPÄNNINGSGENOMFÖRING (10 kV)
c) " " NEDRE ELEKTRODHÅLLARE (⏚)
d) " " GASVENTIL (IN)
e) " " " (UT)
f) " " DETALJ NR 7
g) STÖDBEN

Det.-nr	Ant.	Benämning	Material	Mod.-nr Ämne Dimension	Anm.
6	1	CYLINDER	PLEXIGLASS	Ø160/152×300	
6	1	CYLINDER	PLEXIGLAS	Ø160/152×300	

Konstr. | Ritad: mtj | Kop. | Kontr. | Stand. | Godk. | Skala | Ersätter | Ersatt av

DETAIL Nº 6
CYLINDER Ø160

Dat. 1985-05-25
Ritn.-nr 5

Nr	Ant.	Ändring och/eller medd.-nr	Datum	Inf.	Godk.	Nr	Ant.	Ändring och/eller medd.-nr	Datum	Inf.	Godk.

Svenska A3-1,11 SMS 687

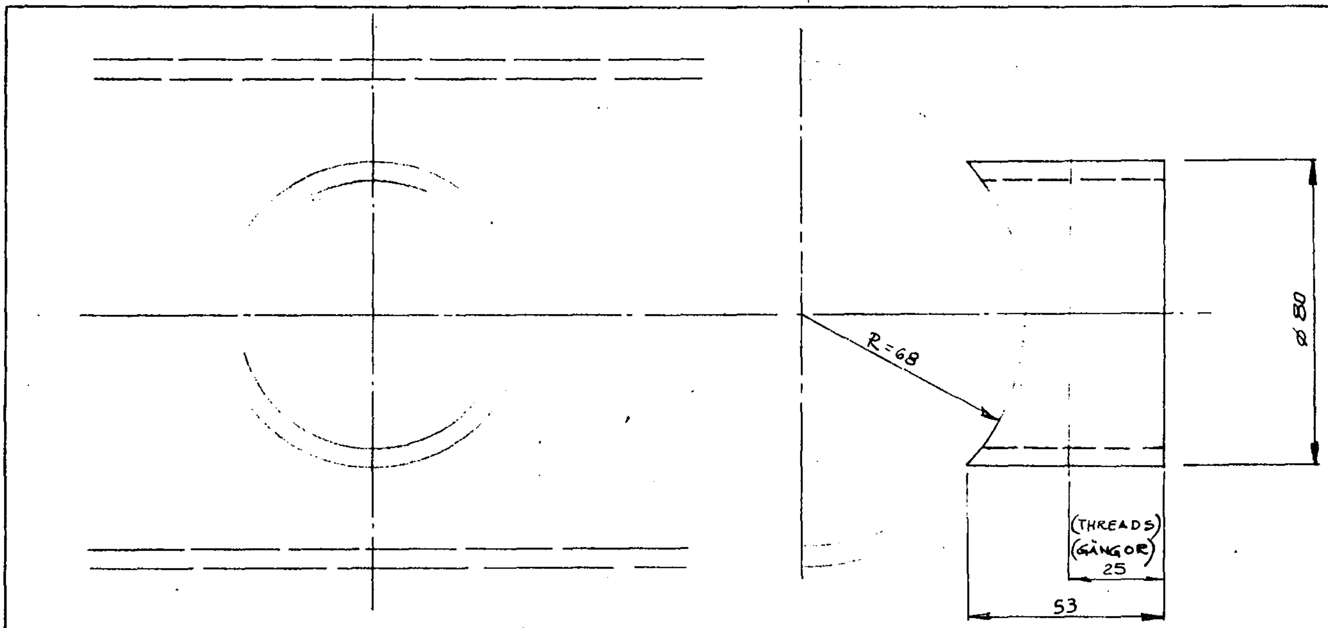

Det.-nr	Ant.	Benämning	Material	Mod.-nr Ämne Dimension	Anm.
7	1	CONNECTING BRANCH	PLEXIGLASS	Ø80/70×53	
7	1	RÖRSTOS	PLEXIGLAS	Ø80/70×53	

Konstr. | Ritad: mtj | Kop. | Kontr. | Stand. | Godk. | Skala | Ersätter | Ersatt av

DETAIL Nº 7
PLEXIGLASS TUBE F ANGULAR

Dat. 1985-05-25
Ritn.-nr 6

Svenska A3-1,11 SMS 687

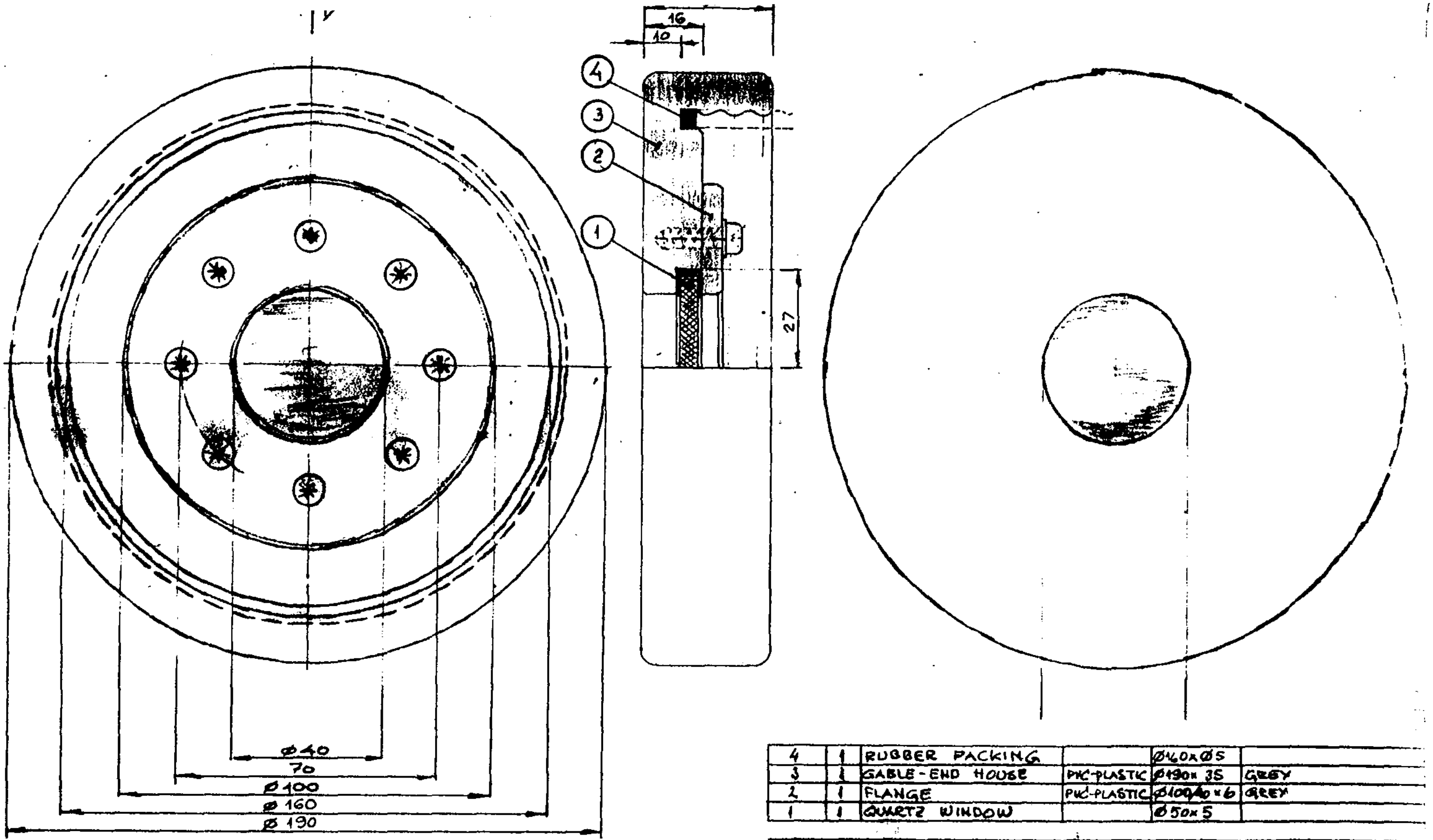

Det.-nr	Ant.	Benämning	Material	Mod.-nr Ämne Dimension	Anm.
4	1	RUBBER PACKING		Ø40xØ5	
3	1	GABLE-END HOUSE	PVC-PLASTIC	Ø190x 35	GREY
2	1	FLANGE	PVC-PLASTIC	Ø100/40x6	GREY
1	1	QUARTZ WINDOW		Ø50x5	
4	1	GUMMITÄTNING		Ø160xØ5	
3	1	GAVELHUS	PVC-PLAST	Ø190	GRÅ
2	1	PRESSFLÄNS	PVC-PLAST	Ø100/40x6	GRÅ
1	1	KVARTSGLAS-SKIVA		Ø80x5	

Konstr.	Ritad	Kop.	Kontr.	Stand.	Godk.	Skala	Ersätter	Ersatt av
	mtj							

DETAIL Nº 8, Ø160

GABLE-END HOUSE

Dat. 1985-06-25

Ritn.-nr 7

Nr	Ant.	Ändring och/eller medd.-nr	Datum	Inf.	Godk.	Nr	Ant.	Ändring och/eller medd.-nr	Datum	Inf.	Godk.

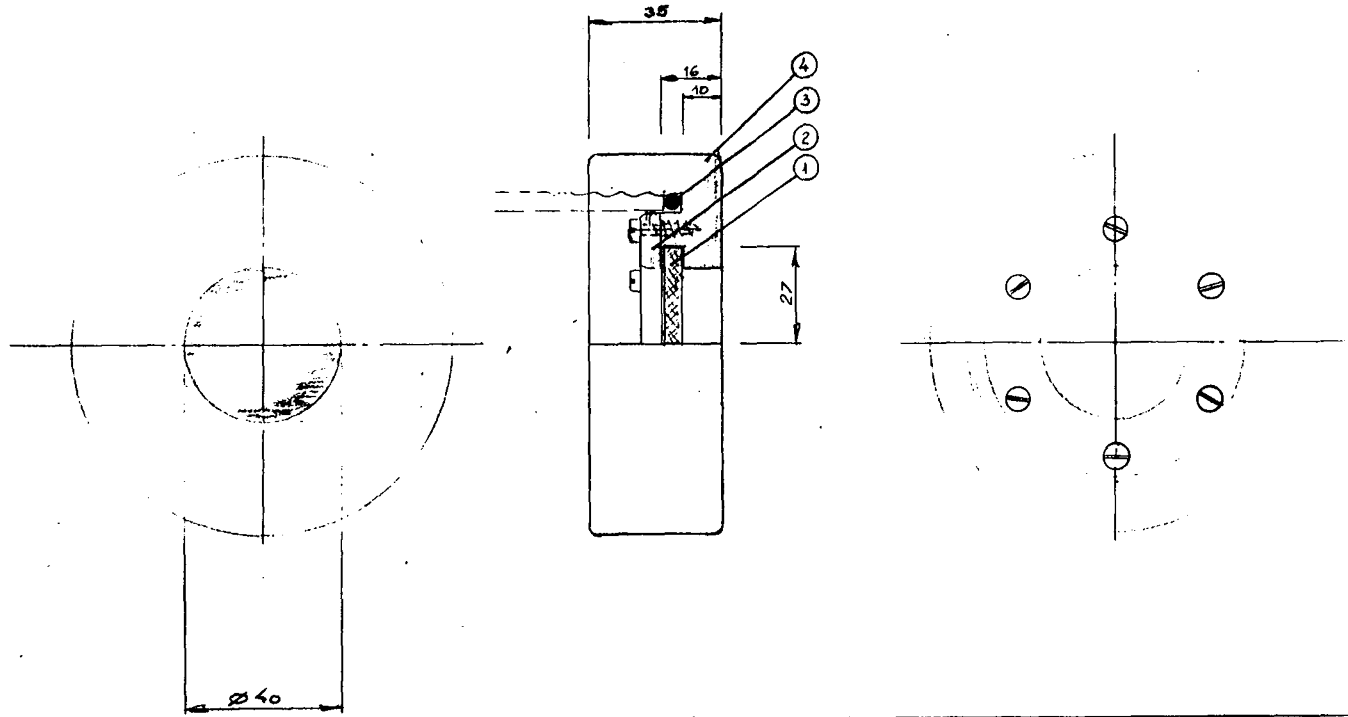

Det.-nr	Ant.	Benämning	Material	Mod.-nr Ämne Dimension	Anm.
4	1	GABLE-END HOUSE	PVC-PLASTIC	Ø100x 35	GREY
3	1	RUBBER PACKING		Ø75xØ5	
2	1	FLANGE	PVC-PLASTIC	Ø68/40x6	GREY
1	1	QUARTZ WINDOW		Ø50x5	
4	1	GAVELHUS	PVC-PLAST	Ø100x 35	GRÅ
3	1	GUMMITÄTNING		Ø75xØ5	
2	1	PRESSFLÄNS	PVC-PLAST	Ø68/40x6	GRÅ
1	1	KVARTSGLAS-SKIVA		Ø50x5	

Konstr.	Ritad	Kop.	Kontr.	Stand.	Godk.	Skala	Ersätter	Ersatt av
	mtj							

DETALJ Nº 9, Ø80

GABLE-END HOUSE

Dat. 1985-05-

Ritn.-nr 8

Nr	Ant.	Ändring och/eller medd.-nr	Datum	Inf.	Godk.	Nr	Ant.	Ändring och/eller medd.-nr	Datum	Inf.	Godk.

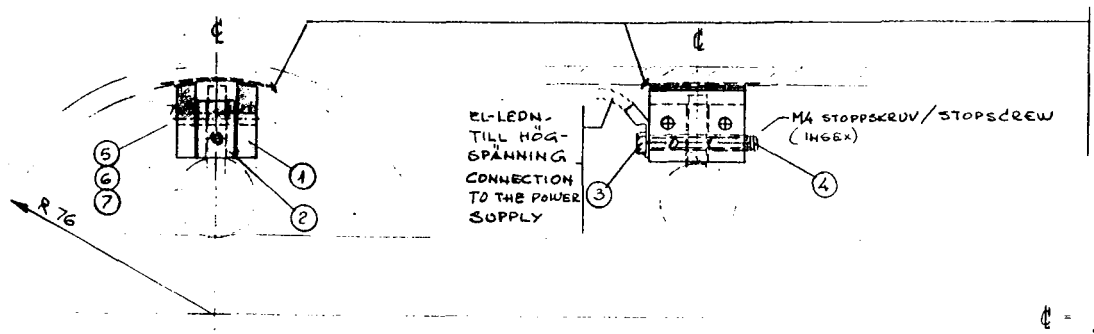

YTA SOM SKA RUGGAS UPP, FÖRE LIMNINGEN MED EPOXILIM

SURFACE IS TO BE BUFFED BEFORE GLUEING WITH EPOX GLUE

℄ = OBSERVATIONSGLASETS CENTRUMLINJE

CENTRE AXIS OF QUART. WINDOW

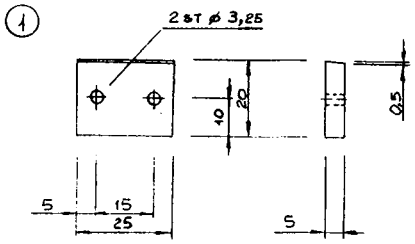

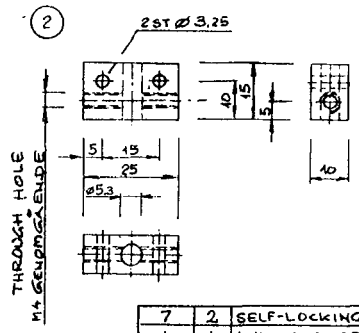

7	2	SELF-LOCKING NUT	STEEL	M3	
6	4	NUT WASHER	STEEL	Ø3,2	
5	2	ASSEMBLY SCREW	STEEL	M3×25	
4	1	CLAMPING SCREW	STEEL	M4×12	
3	1	CONTACT SCREW	STEEL	M4×10	
2	1	ELECTRODE HOLDER	STEEL	15×10×25	YELLOW CHROMATED
1	2	BACKING PLATE	PLEXIGLASS	25×20×5	

7	2	SJÄLVLÅS. MUTTER	STÅL	M3	LOCKING
6	4	BRICKA	STÅL	Ø3,2	
5	2	MONTAGESKRUV	STÅL	M3x 25	
4	1	STOPPSKRUV	STÅL	M4x 12	
3	1	KONTAKTSKRUV	STÅL	M4x 10	
2	1	ELEKTRODHÅLLARE	STÅL	15×10×25	GULKROMATERAD
1	2	FÄSTBRON	PLEXIGLAS	25×20×5	
Del.-nr	Ant.	Benämning	Material	Mod.-nr Ämne Dimension	Anm.

Konstr. mtj Kop. Kontr. Ritad Godk. Skala Ersätter Ersatt av

DETAIL Nr 10
UPPER ELECTRODE HOLDER

Datum 1985-05-2
Ritn.-nr 9

Nr	Ant.	Ändring och/eller medd.-nr	Datum	Inf.	Godk.	Nr	Ant.	Ändring och/eller medd.-nr	Datum	Inf.	Godk.

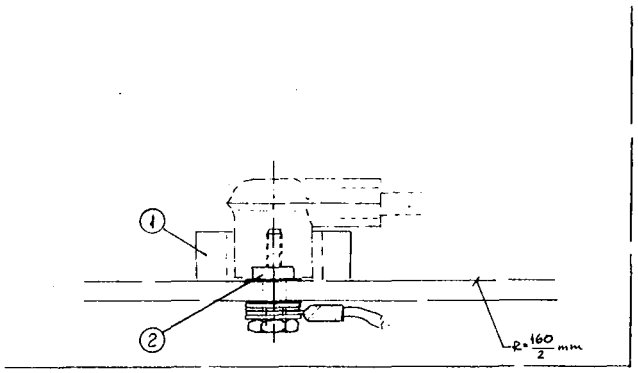

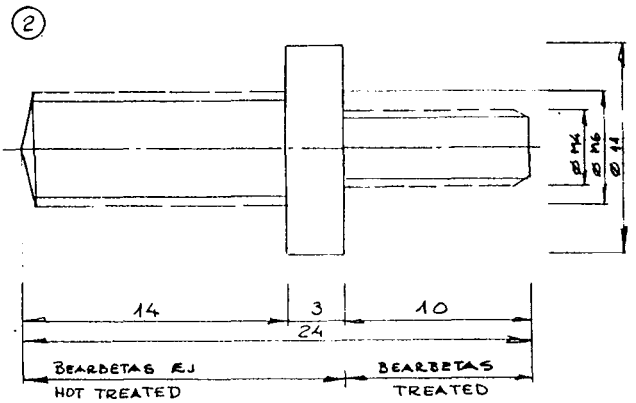

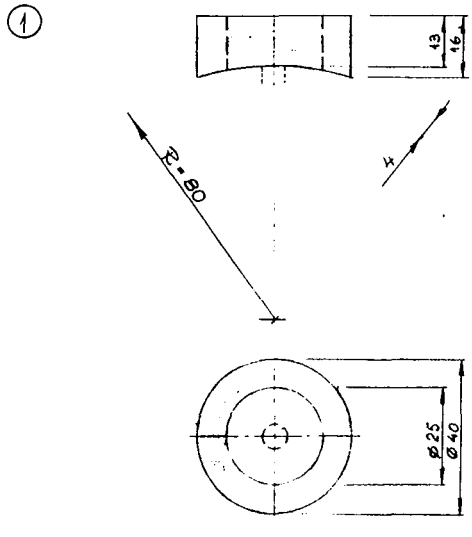

2	1	THROUGH PASS PIN	BRASS		SEMI-MANUFACTURE
1	1	SEMI PROTECTION	PLEXIGLASS	Ø40/25×16	

2	1	GENOMFÖR.-STIFT	MÄSSING		HALVFABRIKAT
1	1	BERÖRINGSSKYDD	PLEXIGLAS	Ø40/25×16	
Del.-nr	Ant.	Benämning	Material	Mod.-nr Ämne Dimension	Anm.

Konstr. mtj Kop. Kontr. Ritad Godk. Skala 1:1 Ersätter Ersatt av

DETAIL Nr 11
HIGH TENSION THROUGH PASS

Datum 1985-05-25
Ritn.-nr 10

Nr	Ant.	Ändring och/eller medd.-nr	Datum	Inf.	Godk.	Nr	Ant.	Ändring och/eller medd.-nr	Datum	Inf.	Godk.

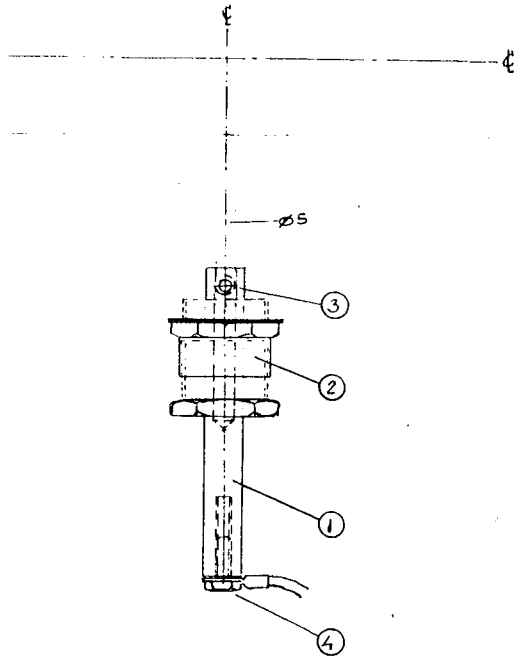

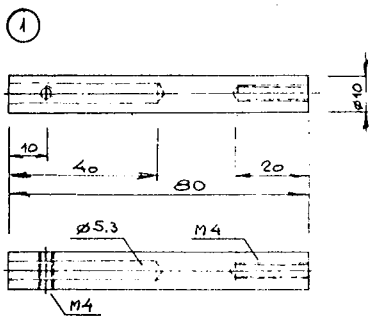

4	1	CONTACT SCREW	STEEL	M4 x 12	
3	1	CLAMPING SCREW	STEEL	M4 x 10	
2	1	COMPRESSION GLAND	″	22,5 (Pg 16)	
1	1	ELECTRODE HOLDER	STEEL	Ø10 x 80	YELLOW CHROMATED

4	1	KONTAKTSKRUV	STÅL	M4 x 12	
3	1	STOPPSKRUV (INSEX)	STÅL	M4 x 10	
2	1	TÄTNINGSHYLSA	″	22,5 (Pg 16)	Elbmutschon
1	1	ELEKTRODHÅLLARE	STÅL	Ø10 x 80	GULKROMATERAS
Det.-nr	Ant.	Benämning	Material	Mod.-nr Ämne Dimension	Anm.

Konstr. mtj Kop. Kontr. Standr. Godk. Skala Gruppbeteckning Ersatt av

DETAIL Nº 12
LOWER ELECTRODE HOLDER

Ritn.-nr 11 Dat. 1985-05-25

Nr	Ant.	Ändring och/eller medd.-nr	Datum	Inf.	Godk.	Nr	Ant.	Ändring och/eller medd.-nr	Datum	Inf.	Godk.

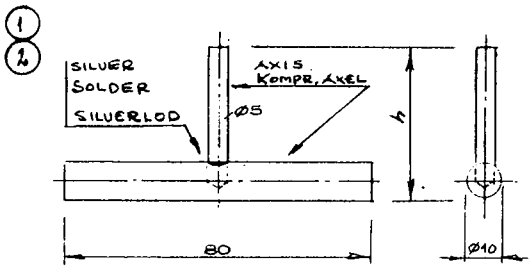

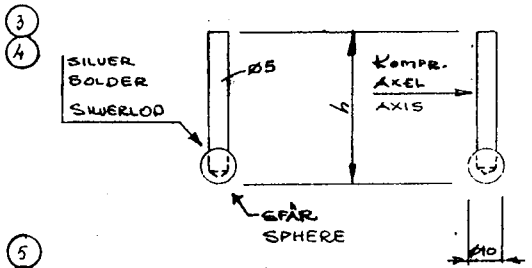

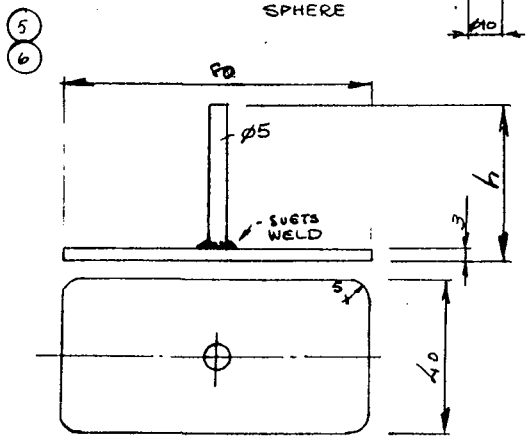

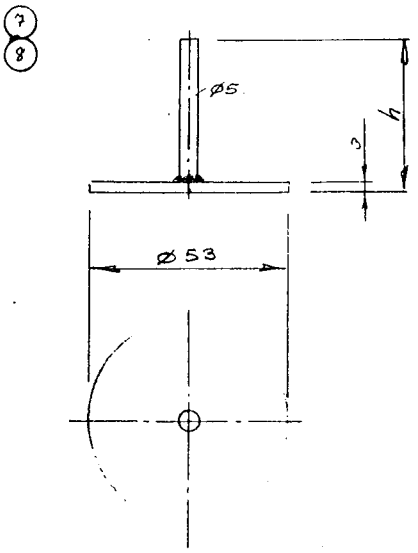

8	1	CIRCLE, LOWER	STEEL		h = 80
7	1	CIRCLE, UPPER	STEEL		h = 60
6	1	RECTANGLE, LOWER	STEEL		h = 80
5	1	RECTANGLE, UPPER	STEEL		h = 60
4	1	SPHERE, LOWER	STEEL		h = 80
3	1	SPHERE, UPPER	STEEL		h = 60
2	1	CYLINDER, LOWER	STEEL		h = 80
1	1	CYLINDER, UPPER	STEEL		h = 60

8	1	CIRKEL, NEDRE	STÅL		h = 80
7	1	CIRKEL, ÖVRE	STÅL		h = 60
6	1	REKTANGEL, NEDRE	STÅL		h = 80
5	1	REKTANGEL, ÖVRE	STÅL		h = 60
4	1	SFÄR, NEDRE	STÅL		h = 80
3	1	SFÄR, ÖVRE	STÅL		h = 60
2	1	CYLINDER, NEDRE	STÅL		h = 80
1	1	CYLINDER, ÖVRE	STÅL		h = 60
Det.-nr	Ant.	Benämning	Material	Mod.-nr Ämne Dimension	Anm.

Konstr. mtj Kop. Kontr. Standr. Godk. Skala Gruppbeteckning Ersatt av

ELECTRODES

Ritn.-nr 12 Dat. 1985-05-25

Nr	Ant.	Ändring och/eller medd.-nr	Datum	Inf.	Godk.	Nr	Ant.	Ändring och/eller medd.-nr	Datum	Inf.	Godk.